Scanning electrochemical microscopy in the 21st century†

Peng Sun, François O. Laforge and Michael V. Mirkin

Received 25th August 2006, Accepted 14th November 2006
First published as an Advance Article on the web 30th November 2006
DOI: 10.1039/b612259k

The fundamentals of and recent advances in scanning electrochemical microscopy (SECM) are described. The focus is on applications of this method to studies of systems and processes of active current interest ranging from nanoelectrochemistry to electron transfer reactions and electrocatalysis to biological imaging.

1. Introduction

The invention of the scanning tunneling microscope in early 1980s[1] almost coincided with the introduction of micron-sized ultramicroelectrodes (UMEs).[2] Since that time, the idea of scanning electrochemical microscopy (SECM; the same abbreviation is also used for the device, *i.e.*, the microscope) was in the air. Several groups employed small and mobile electrochemical probes to make measurements within the diffusion layer,[3] examine and modify electrode surfaces.[4,5] However, the SECM technique, as we know it, only became possible after the introduction of the feedback concept.[6,7]

Fig. 1 shows the temporal distribution of the SECM-related articles published since 1986. The data for this figure was taken from Wipf's comprehensive online SECM bibliography.[8] Two distinctly different periods can be identified in Fig. 1: an "induction period" (from 1986 to ~1994), when the number of publications was relatively small, but the most important theoretical and experimental methodology was developed; and a subsequent period of explosive growth. The number of research groups employing SECM increased dramatically after the first commercial instrument was offered by CH Instruments in 1999. Hence, more than 50% of the SECM publications appeared within the last five–six years. Because those articles have not been surveyed in the SECM monograph published in 2001,[9] the objective of this review is to give a brief summary of advances in the field reported since the year 2000. The comparison of the volume of this article to that of ref. 9 shows that our survey is necessarily incomplete.

SECM is a powerful tool for studying structures and processes in micrometer- and submicrometer-sized systems. It can probe electron, ion, and molecule transfers, and other reactions at solid-liquid, liquid–liquid, and liquid-air interfaces.[10] This versatility allows for the investigation of a wide variety of processes, from metal corrosion to adsorption to metabolism in single living cells, as discussed below in the Applications section.

SECM employs an UME probe ("tip") to induce chemical changes and collect electrochemical information while approaching or scanning the surface of interest ("substrate"). The substrate may also be biased and serve as the second working electrode. Many different types of UMEs have been fabricated, *e.g.*, microband electrodes, cylindrical electrodes, microrings, disk-shaped, and hemispherical electrodes.[11,12] For reasons discussed below, the disk geometry is preferred for SECM tips, though other shapes may be suitable for specific experiments.[13–20] UMEs offer important advantages for electroanalytical applications including greatly diminished ohmic potential drop in solution and double-layer charging current, the ability to reach a steady state in seconds or milliseconds, and a small size allowing one to do experiments in microscopic domains.

The precise positioning capabilities, which make high spatial resolution possible, give the SECM an important edge over other electrochemical techniques employing UMEs.[21] For example, the SECM can pattern the substrate surface, visualize its topography, and probe chemical reactivity on the micrometer or nanometer scale. At the same time, SECM differs from other SPM techniques in its applicability to quantitative measurements (*e.g.*, kinetic experiments) through well-developed and rigorous electrochemical theory. The nature of the tip and the way it interacts with the substrate determine what information can be obtained in an SECM experiment. Here, we briefly survey the fundamentals of

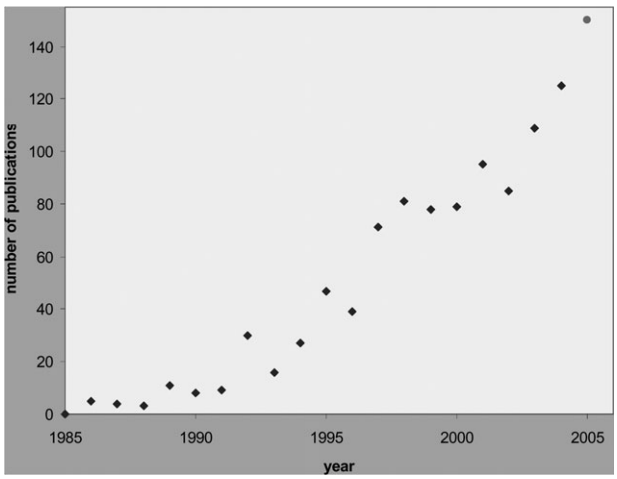

Fig. 1 The number of the SECM-related articles published over the last twenty years. The last dot is an estimate based on the data available for 2005 in ref. 8.

Department of Chemistry & Biochemistry, Queens College–CUNY, Flushing, NY 11367, USA
† The HTML version of this article has been enhanced with additional colour images.

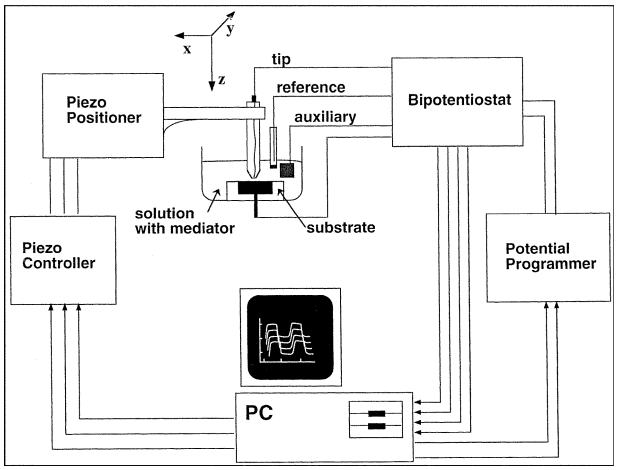

Fig. 2 Block diagram of the SECM apparatus. (Reprinted with permission from ref. 62. Copyright 1991, American Association for the Advancement of Science.)

various modes of the SECM operation and then focus on more recent advances in SECM theory and applications.

2. Principles of SECM operation

Fig. 2 shows a schematic diagram of the basic SECM instrument employing an amperometric microprobe. An UME tip is attached to a 3D piezo positioner controlled by a computer, which is also used for data acquisition. A bipotentiostat (*i.e.*, a four-electrode potentiostat) controls the potentials of the tip and/or the substrate *versus* the reference electrode and measures the tip and substrate currents. The SECM instrument is often mounted on a vibration-free optical table inside a Faraday cage to isolate it from environmental vibrations and electromagnetic noise—this is especially important for high-resolution (nm-scale) and low-current (pA and sub-pA) measurements. With essentially the same setup, several SECM modes of operation can be realized including feedback mode, tip generation/substrate collection (TG/SC) mode, substrate generation/tip collection (SG/TC) mode, penetration mode and ion transfer feedback mode.

2.1. Feedback mode

In a feedback mode experiment, the tip is immersed in a solution containing a redox mediator (*e.g.*, an oxidizable species, R). When a sufficiently positive potential is applied to the tip, the oxidation of R occurs *via* the reaction

$$\mathrm{R} - ne^- \rightarrow \mathrm{O} \qquad (1)$$

at a rate governed by diffusion of R to the UME surface. If the tip is far (*i.e.*, greater than several tip diameters) from the substrate (Fig. 3A) the steady-state current, $i_{T,\infty}$, is given by

$$i_{T,\infty} = 4nFDca \qquad (2)$$

where F is the Faraday constant, n is the number of electrons transferred in reaction (1), D and c are the diffusion coefficient and the bulk concentration of R, respectively, and a is the tip radius.

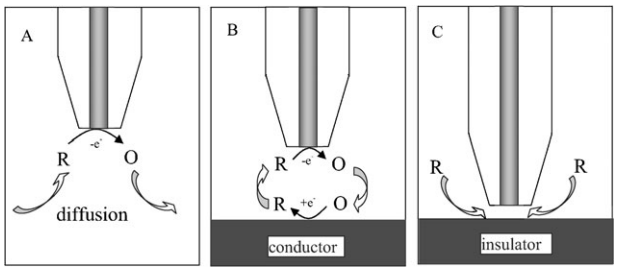

Fig. 3 Feedback mode of the SECM operation. (A) The UME tip is far from the substrate. (B) Positive feedback: species R is regenerated at the substrate. (C) Negative feedback: diffusion of R to the tip is hindered by the substrate.

When the tip is brought to within a few tip radii of a conductive substrate surface (Fig. 3B), the O species formed in the reaction (1) diffuses to the substrate where it can be reduced back to R

$$\mathrm{O} + ne^- \rightarrow \mathrm{R} \qquad (3)$$

This process produces an additional flux of R to the tip and hence "positive feedback", *i.e.*, the increase in tip current ($i_T > i_{T,\infty}$). The shorter the tip-substrate separation distance (d), the larger the tip current. When reaction (3) is rapid, $i_T \rightarrow \infty$ as $d \rightarrow 0$.

If the substrate is an inert electrical insulator, the tip-generated species, O, cannot react at its surface. At small d, $i_T < i_{T,\infty}$ because the insulator blocks the diffusion of species R to the tip surface ("negative feedback"; Fig. 3C). The closer the tip to the insulator substrate, the smaller the i_T, with $i_T \rightarrow 0$ as $d \rightarrow 0$. Overall, the rate of the mediator regeneration at the substrate determines the magnitude of the tip current, and conversely the measured i_T *vs.* d dependence ("approach curve") provides information on the kinetics of the process at the substrate.

If the substrate is a conductor, rate of reaction (3) can be controlled by applying a suitable potential to it by a potentiostat. Alternatively, the potential of a conductive substrate (E_s) may be determined by concentrations of redox species in solution without an external bias. For example, if the solution contains only the reduced form of the redox species, most of the substrate surface (which is usually much larger than that of the tip) is exposed to solution of R. According to the Nernst equation

$$E_s = E^\circ + \frac{RT}{nF}\ln\frac{c_O}{c_R} \qquad (4)$$

In this case, $c_O \sim 0$, and $E_s - E^\circ \ll 0$, where E° is the standard potential of the mediator, and all oxidized species reaching the substrate get reduced at its surface.

2.2. Tip generation/substrate collection

In the tip generation/substrate collection mode (TG/SC) experiment, the tip generates an electroactive species that diffuses across the tip/substrate gap to react at the substrate surface (Fig. 4A). A TG/SC experiment includes simultaneous measurements of both tip and substrate currents (i_T and i_S).

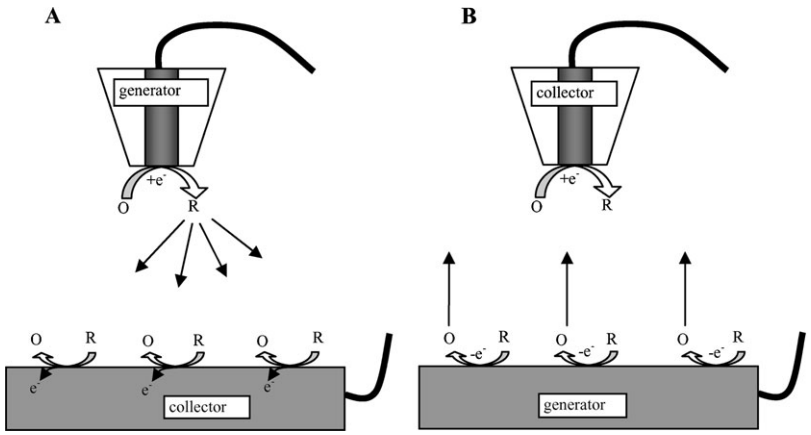

Fig. 4 Scheme of TG/SC mode (A) and SG/TC mode (B). (A) The tip generates species R by reduction of O in solution; R diffuses toward the substrate and is reoxidized to O. (B) O is electrogenerated at the substrate surface and collected at the tip. The tip and substrate currents are recorded in both cases.

For a one-step heterogeneous electron transfer (ET) at steady state, these quantities are almost identical if d is not very large, and consequently the collection efficiency, $i_S/i_T > 0.99$ at $d \leq 2a$. Under these conditions, the tip-generated species, R predominantly diffuse to the large substrate, rather than escape from the tip-substrate gap. For a process with a coupled homogeneous chemical reaction, there may be large differences between i_s and i_T, and both quantities can provide important kinetic information. For instance, species R may undergo a first order irreversible reaction whose product is electrochemically inactive. If the reaction is slow, the process is diffusion-controlled, the i_T *vs.* d curves follow the positive feedback theory, and $i_s/i_T \rightarrow 1$ at short separation distances. In contrast, if homogeneous reaction is very fast, most species R get converted to the electroinactive product before reaching the substrate. Hence, the very low substrate current, and $i_s/i_T \rightarrow 0$. Between these two extreme cases, the homogeneous kinetics can be determined by measuring the collection efficiency as a function of d.[22–26]

TG/SC can also be used to induce a transient equilibrium perturbation. The tip process modifies the local concentration of a redox species which affects the chemical equilibrium at the substrate surface. The dynamics of the perturbation response and the recovery after the perturbation can be monitored by recording the tip current as a function of time. An application of this method is discussed in section 5.2.

2.3. Substrate generation/tip collection mode

Historically, the first SECM-type experiments were carried out to measure concentration profiles in the diffusion layer generated by a macroscopic substrate.[3] This type of measurement represents substrate generation/tip collection (SG/TC) mode. When the tip is moved through the thick diffusion layer produced by the substrate, the changes in i_T reflect local variations of concentrations of redox species (Fig. 4B). Ideally, the tip should not perturb the diffusion layer at the substrate. This is easier to achieve with a potentiometric tip, which is a passive sensor and does not change concentration profiles of electroactive species. The higher resolution in such experiments can be achieved and the concentration profile perturbation can be minimized by using nanometer-sized tips, as shown by Amatore, Heinze *et al.*[27]

The collection efficiency in SG/TC mode is much lower than that in the TG/SC mode, and the true steady state can be achieved only by using a micrometer-sized substrate. Other disadvantages of this mode are the high sensitivity to noise and the difficulty in controlling the tip/substrate separation distance.

Theoretical treatments for SG/TC mode have been reported for a spherical cap or an embedded microdisk-shaped substrate that generates stable species and for a smaller tip collecting them.[28–33] This mode can be used for monitoring corrosion, enzymatic reactions, and other heterogeneous processes at the substrate surface.

2.4. Penetration experiments

In this mode, a small SECM tip is used to penetrate a microstructure, *e.g.*, a submicrometer-thick polymer film containing fixed redox centers or loaded with a redox mediator, and extract spatially resolved information (*i.e.*, a depth profile) about concentrations, kinetic and mass-transport parameters.[34,35] With a tip inside the film, relatively far from the underlying conductor or insulator, solid-state voltammetry at the tip can be carried out similarly to conventional voltammetric experiments in solution. At smaller distances, the tip current either increases or decreases depending on the rate of the mediator regeneration at the substrate. If the film is homogeneous and not very resistive, the current-distance curves are similar to those obtained in solution.

More recent penetration experiments were carried out in biological systems, *i.e.*, large intact nuclei,[36] giant liposomes,[37] and mammalian cells.[38] Such experiments can provide information about the distribution of electroactive species inside the cell, potentials, and ion transfers across biological membranes (see section 5.5).

2.5. Electron-transfer and ion-transfer feedback experiments at the liquid/liquid interface

Heterogeneous charge-transfer reactions at the interface between two immiscible electrolyte solutions (ITIES) and

liquid-membrane interfaces are of fundamental importance for many biological and technological systems. When SECM is used to probe ET at the ITIES, an UME tip is placed in the upper liquid phase (*e.g.*, organic solvent) containing one form of the redox species (*e.g.*, the reduced form, R_1). With the tip held at a sufficiently positive potential, R_1 reacts at the tip surface to produce the oxidized form of the species, O_1. When the tip approaches the ITIES, the mediator can be regenerated at the interface *via* the bimolecular redox reaction between O_1 in the organic phase (o) and R_2 in the aqueous phase (w)

$$O_1(o) + R_2(w) \rightarrow R_1(o) + O_2(w) \qquad (5)$$

and i_T increases with the decrease in d (positive feedback). The kinetics of such a reaction can be evaluated from approach curves.

The ion-transfer feedback mode can also be used to probe the transfers of electroinactive ionic species, *e.g.*, ClO_4^-, alkali metal cations, and tetraalkylammonium cations across the ITIES. A micrometer- or nanometer-sized pipette can be filled with a solvent immiscible with the outer solution and used as a tip to approach a macroscopic ITIES (Fig. 5). In an SECM study of facilitated ion transfer,[39] the transfer of K^+ from aqueous filling solution to the external 1,2-dichloroethane solution was assisted by dibenzo-18-crown-6 (DB18C6).

$$K^+_{(w)} + DB18C6_{(DCE)} \rightarrow [KDB18C6]^+_{(DCE)} \qquad (6a)$$
(at the pipette tip)

With the tip biased at an appropriate potential and the concentration of KCl inside the pipette much higher than the concentration of DB18C6 in DCE, the current was limited by the diffusion of DB18C6 to the pipette orifice. When the tip approached the ITIES, the regeneration of DB18C6 occurred *via* an interfacial dissociation mechanism

$$[KDB18C6]^+_{(DCE)} \rightarrow K^+_{(w)} + DB18C6_{(DCE)} \qquad (6b)$$
(at the ITIES)

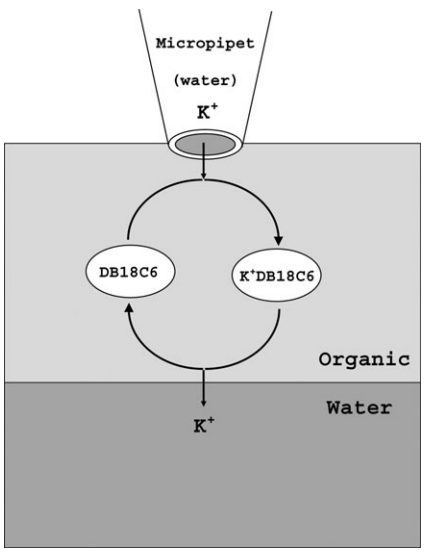

Fig. 5 Schematic diagram of the feedback mode of facilitated ion-transfer reaction.

and a positive feedback current was observed. Positive feedback can also be produced by a simple ion transfer reaction.[40]

In most SECM experiments, a non-polarizable ITIES was poised by the concentrations of the potential-determining ion providing a constant driving force for either ET or ion transfer process. Alternatively, a polarizable ITIES can be externally biased.[41] In this case, the applied interfacial voltage should be within the polarization window, where almost no current flows across a macroscopic liquid–liquid interface. The tip reaction changes the concentrations of redox species in a thin layer near the phase boundary and induces a small current across a micrometer-sized portion of the ITIES. An advantage of such an approach is in a potentially wider range of interfacial voltages available for the ET study (as compared to those at a non-polarizable interface).

Because of the volume limitations, we cannot offer a more detailed discussion of SECM experiments at the liquid–liquid interface in this article. Several reviews of this subject are available.[10,42] More recent publications describe the studies of ET at the water/ionic liquid interface;[43] observations of inverted Marcus behavior at the ITIES;[44] ET between molecules and nanoparticles confined to different liquid phases;[45,46] probing facilitated ion transfer across an externally polarized ITIES;[47] and the study of phase-transfer processes by combination of the SECM with a Langmuir trough.[48]

3. Instrumentation

3.1. Tip

A typical SECM probe is a micrometer-sized UME sharpened to allow closer approach to the substrate surface.[6] Such probes are easy to fabricate from commercially available microwires and polish, thus ensuring accuracy and reproducibility of their electrochemical responses. An established procedure involves heat sealing of a microwire or a carbon fiber in a glass capillary under vacuum and connecting it with silver epoxy to a larger copper wire on the back side.[6] The sealed side of the probe is polished down to 50 nm alumina and then sharpened to form a tip using coarse sandpaper. The important parameters of the tip geometry are (1) the radius of the conductive core, a; and (2) the total tip radius (*i.e.*, a plus the insulating sheath thickness), r_g. The dimensionless parameter $RG = r_g/a$ is normally ≤ 10. This fabrication method does not require any expensive equipment, and it is widely used for the production of micron-sized tips. Alternatively, one can use electrophoretic paint as an insulator for microwires. Ciani and Daniele reported extensive electrochemical characterization of the SECM tips produced by this method.[49]

Nanometer- and submicrometer-sized tips have been fabricated differently. A simple way to produce nanometer-sized conical electrodes consists in etching a metal wire and then coating it with an insulator while leaving the apex exposed. For example, a 250-μm-diameter Pt-Ir wire was etched in a solution containing 3 M NaCN and 1 M NaOH by applying a 20 V ac between the wire and the solution. Then, it was insulated by dipping the metal tip into molten Apiezon wax, and finally its very end was exposed by using an STM.[50] Many more types of coating have been tried such as varnish, molten

paraffin, silica coating, poly(α-methylstyrene), polyimide,[51] electropolymerized phenol, and electrophoretic paint.[52] Submicrometer-sized conical carbon tips were prepared by Zhan and Bard using flame etching.[37]

Most nanotips prepared by etching are conical and not polishable.[13,50–53] Such tips are suitable for high resolution imaging and penetration experiments, but they are less useful for quantitative kinetic measurements and especially for feedback mode experiments. Disk-type tips can be prepared using a micropipette puller.[54–56] Shao *et al.* used a laser puller to prepare glass-sealed Pt electrodes with radii ranging from 2 to 500 nm.[55] They attempted to polish larger (>100 nm) electrodes and to characterize the tip geometry by combination of SEM, steady-state voltammetry and SECM; but the quality of the obtained approach curves was not high. A somewhat different approach to polishing of pulled submicrometer electrodes was proposed by Katemann and Schuhmann.[56] Recently, it was shown that a tip as small as ~10-nm-radius can be polished on a lapping tape under the video-microscopic control.[54] The polished flat nano-tips yield more reliable and reproducible data, and can be used for fast kinetic measurements.

The addition of an electromagnetic shield to the body of the tip can greatly reduce the stray capacitance. This is particularly useful for fast-scan voltammetry[57] and high-frequency impedance experiments.[58]

3.2. Positioning

Similarly to other scanning probe microscopies, an SECM probe has to be moved in *x*-, *y*-, and *z*-directions with a nanometer-scale precision. However, the required travel distance can be as long as a few hundred microns. Most of SPM positioning devices are not suitable for such long scans. Also, a reasonable accuracy in the *x*- and *y*- directions has to be combined with a higher accuracy in *z*-direction for the measurement of i_T *vs.* *d* curves. One possibility is to use inchworm motors for *x*- and *y*-axes traveling and for relatively coarse *z*-scans, while a vertical PZT piezo pusher is used for finer *z*-control over short distances. Inchworm motors use a clamping mechanism that produces slight lateral and possibly axial discontinuities of the displacement every 2 microns of travel when the axis is clamped/unclamped. The lateral motion discontinuity can be eliminated by using the motor to drive a ball bearing linear stage on which the probe is attached. However, the axial discontinuity can be fatal for nanotips, as a crash could occur if the tip is close to the substrate when clamping/unclamping. Other combinations are possible, for example the CHI900B SECM (CH Instruments Inc.) uses stepper motors for coarse positioning and a XYZ piezo block for finer displacements which gives an overall resolution of 1.6 nm. Close-loop positioners with position sensors such as optical encoders, capacitive sensors or strain gauge sensors offer the possibility to precisely reposition the tip. An interesting advantage of the repositioning capability is the possibility of mapping–and recording–the topography of the surface and subsequently scanning the same area at constant distance to the surface to deconvolute the contributions of surface topography and reactivity to the tip current.

Unlike STM and AFM tips, which are sharp cones, a typical SECM tip is a conductive disk surrounded by the flat ring of insulating glass whose thickness is equivalent to several disk radii. Thus, a proper alignment of the tip with respect to the substrate surface is crucial. Unless the tip surface is flat and strictly parallel to the substrate plane, the insulator touches the substrate first and prevents the conductive disk from coming close to its surface. To facilitate the alignment, special care must be given to the attachment of the tip to the translation stage and to substrate mounting (see also section 4.2.2).

3.3. Potentiostat

Many SECM experiments require biasing the substrate. A bipotentiostat in Fig. 2 is used to control both the tip and substrate potentials. Unless transient measurements are made, the response of the bipotentiostat does not have to be fast. More importantly, it should be capable of measuring a broad range of current responses: a pA scale (or even sub-pA) tip current and a much higher current at a macroscopic substrate. For this reason, it is convenient to have several choices of preamplifiers/current-to-voltage transducers.

4. Theory

The quantitative SECM theory has been developed for various heterogeneous and homogeneous processes and different tip and substrate geometries. In general, theoretical SECM dependencies can be generated by numerically solving partial differential equations. In some cases, analytical approximations allow for easier generation of theoretical dependencies and analysis of experimental data. Several previous reviews focused on various aspects of the SECM theory.[59–62] Most theoretical results surveyed below concern the SECM with a disk-shaped tip. Some recent theoretical treatments of non-disk tips (*e.g.*, shaped as a cone or a spherical cap) are discussed in section 4.2.1.

4.1. Analytical approximations for steady-state responses

The SECM diffusion problems were solved for both transient and steady-state feedback experiments. Since transient SECM measurements typically are somewhat less accurate and harder to perform, most quantitative studies were carried out under steady-state conditions. The non-steady-state SECM response depends on too many parameters to allow presentation of a complete set of working curves that would cover all experimental possibilities. The steady-state theory is simpler and often can be expressed in the form of dimensionless working curves or analytical approximations.

4.1.1. Diffusion-controlled heterogeneous reactions. The dimensionless steady-state current-distance curves were calculated numerically by Kwak and Bard[7] for both pure positive and negative feedback conditions assuming a diffusion-controlled mediator turnover, equal diffusion coefficients, and an infinitely large substrate (the current–distance curves for microscopic substrates can be found in ref. 63).

Several previously published analytical expressions for the current *vs.* distance curve for pure positive feedback and different RG values were recently discussed by Lefrou.[64]

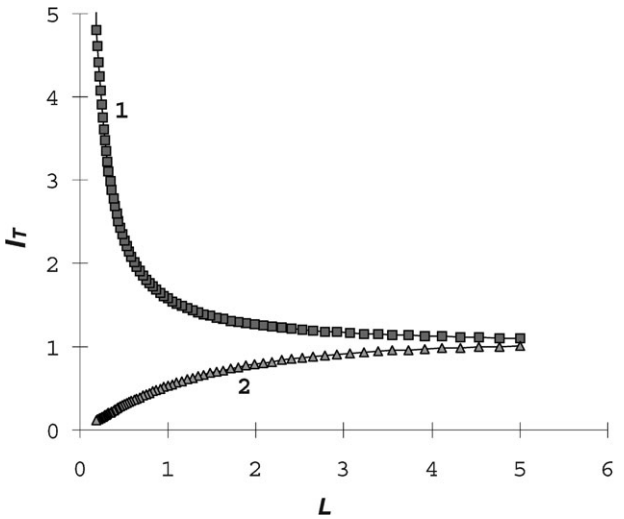

Fig. 6 Theoretical approach curves for a tip electrode over a conductive (1) and insulating (2) substrate. Solid lines are computed for RG = 10 from eqn (7) (curve 1) and eqn (8) (curve 2). Symbols are from simulations in ref. 7.

For RG = 10, eqn (7)[13]

$$I_T^C(L) = \frac{i_T}{i_{T,\infty}} = 0.78377/L + 0.3315\exp(-1.0672/L) + 0.68 \quad (7)$$

where $L = d/a$ is the normalized tip/substrate distance, fits the I_T *vs.* L curve over the L interval from 0.05 to 20 to within 0.7% (Fig. 6, curve 1). Since the shape of the approach curve at a conductive substrate does not depend strongly on RG, eqn (7) is sufficiently accurate when the insulating sheath of the tip is not very thin (*e.g.*, RG $\geq$ 3). For very sharp tips, equations similar to eqn (7) with tabulated parameters are available for several RG values.[40,65] Alternatively, one can use a more complicated analytical approximation from ref. 64, which is reasonably accurate (within 2%) for all RG and L.

In the case of an insulating substrate, the shape of the current-distance curve is much more sensitive to the RG value. Fig. 6 shows an approach curve simulated for RG = 10 (curve 2) and a corresponding curve calculated from eqn (8)[40]

$$I_T^{ins}(L) = \frac{i_T}{i_{T,\infty}} = \frac{1}{A + B/L + C\exp(D/L)} + \frac{EL}{F + L} \quad (8)$$

Eqn (8) with the parameter values listed in Table 1 and eqn (9)[65]

$$I_T^{ins}(L) = 1/[k_1 + k_2/L + k_3\exp(k_4/L)] \quad (9)$$

with the parameter values listed in Table 2 cover reasonably well the entire range of RG from 1.1 to 1000. The accuracy of eqn (8) is $\sim$1%, which is smaller than typical experimental uncertainty. Eqn (9) is not valid for small tip/substrate distances. It is suitable for $L \geq 2$ when RG = 1.11 and $L \geq 0.2$ for any other RG in the table.

By fitting an experimental current-distance curve to the theory eqns (7)–(9), one can determine the zero separation point ($L = 0$), which in turn allows one to establish the distance scale essential for any quantitative SECM measurement.

4.1.2. Finite kinetics at the tip or substrate. For the finite heterogeneous kinetics at the tip and diffusion-controlled mediator regeneration at the substrate, an approximate eqn (10) was recently obtained for I_T as a function of tip potential, E, and L[54]

$$I_T(E,L) = \frac{0.78377}{L(\theta + 1/\kappa)} + \frac{0.68 + 0.3315\exp(-1.0672/L)}{\theta\left[1 + \frac{\pi}{\kappa\theta}\frac{2\kappa\theta+3\pi}{4\kappa\theta+3\pi^2}\right]} \quad (10)$$

where $\kappa = \pi\lambda\exp[-\alpha F(E-E^{\circ\prime})/RT]/(4I_T^c)$, $\theta = 1 + \exp[F(E-E^{\circ\prime})/RT]D_O/D_R$, $E^{\circ\prime}$ is the formal potential, α is the transfer coefficient, $\lambda = k^\circ a/D$, and $I_T^c(L)$ is the normalized tip current for the same L and the diffusion-controlled positive feedback at a conductive substrate, as defined by eqn (7).

At constant L, eqn (10) describes a quasi-reversible steady-state tip voltammogram (if kinetics is fast, $\kappa \to \infty$, and eqn (10) reduces to one for a Nernstian tip voltammogram). Such a curve can be obtained by scanning the potential of the tip while the substrate potential is held constant. Finite element simulations in ref. 54 showed that eqn (10) is more accurate than two somewhat similar expressions derived earlier.

The current-distance curves for an irreversible heterogeneous reaction occurring at the substrate while the tip process is diffusion-controlled can be calculated from eqn (11):[66]

$$I_T(L) = I_S\left(1 - \frac{I_T^{ins}}{I_T^c}\right) + I_T^{ins} \quad (11a)$$

$$I_S = \frac{0.78377}{L(1 + 1/\Lambda)} + \frac{0.68 + 0.3315\exp(-1.0672/L)}{1 + F(L,\Lambda)} \quad (11b)$$

where I_T^c and I_T^{ins} are given by eqns (7) and (8), respectively, and I_S is the kinetically controlled substrate current; $\Lambda = k_f d/D$, k_f is the heterogeneous rate constant (cm/s), and $F(L,\Lambda) = (11/\Lambda + 7.3)/(110 - 40L)$.

Although eqn (11) was derived for a one-step heterogeneous ET reaction, it was shown to be applicable to more complicated substrate kinetics (*e.g.*, liquid–liquid interfacial charge

Table 1 Parameter values for eqn (8)

RG	A	B	C	D	E	F
1.1	1.167 5164	1.030 9985	0.380 0855	−1.701 797	0.346 3761	0.036 7416
1.5	1.003 5959	0.929 4275	0.402 2603	−1.788 572	0.283 2628	0.140 1598
2.0	0.783 8573	0.877 792	0.424 8416	−1.743799	0.163 8432	0.199 3907
10	0.457 1825	1.460 4238	0.431 2735	−2.350 667	−0.145 437	5.576 8952

Table 2 Parameter values for eqn (9)

RG	k_1	k_2	k_3	k_4	% Error	Validity range
1002	0.132 19	3.371 67	0.8218	−2.347 19	<1%	0.3–20
100	0.279 97	3.054 19	0.686 12	−2.7596	<1%	0.4–20
50.9	0.305 12	2.6208	0.667 24	−2.6698	<1%	0.4–20
20.1	0.355 41	2.0259	0.628 32	−2.556 22	<1%	0.4–20
15.2	0.373 77	1.851 13	0.613 85	−2.495 54	<1%	0.4–20
10.2	0.404 72	1.601 85	0.588 19	−2.372 94	<1%	0.4–20
8.13	0.426 76	1.460 81	0.568 74	−2.285 48	<1%	0.4–20
5.09	0.486 78	1.177 06	0.512 41	−2.078 73	<1%	0.2–20
3.04	0.604 78	0.860 83	0.395 69	−1.894 55	<0.2%	0.2–20
2.03	0.76179	0.60983	0.23866	−2.03267	<0.15%	0.2–20
1.51	0.904 04	0.427 61	0.097 43	−3.230 64	<0.7%	0.2–20
1.11	−1.465 39	0.272 93	2.456 48	8.995E-7	<1%	2–20

transfer,[66–68] ET through self assembled monolayers,[69a] and mediated ET in living cells[70–73]). The effective heterogeneous rate constant obtained by fitting experimental approach curves to eqn (11) can be related to various parameters, which determine the rates of those processes, as discussed in the referred publications.

The radius of the portion of the substrate surface participating in the SECM feedback loop can be evaluated as $r \cong a + 1.5d$.[63] Thus, at small tip/substrate distances (*e.g.*, $L \leq 2$), a large substrate behaves as a virtual UME of a size comparable with that of the tip electrode. The SECM allows probing local kinetics at a small portion of the macroscopic substrate with all of the advantages of microelectrode measurements.[11,12] The effective mass-transfer coefficient for SECM is

$$m_o = 4D_o \frac{0.68 + 0.78377/L + 0.3315\ \exp(-1.0672/L)}{\pi a} = \frac{i_T(L)}{\pi a^2 nFc} \quad (12)$$

One can see from eqn (12) that at $L \gg 1$, $m_O \sim D/a$ (as for a microdisk electrode alone), but at $L \ll 1$, $m_O \sim D/d$, which is indicative of the thin-layer cell (TLC) type behavior. By decreasing d, the mass-transport rate can be increased sufficiently for quantitative characterization of fast ET kinetics, while preserving the advantages of steady-state methods, *i.e.*, the absence of problems associated with ohmic drop, adsorption, and charging current.

4.1.3. SG/TC mode. Unlike feedback mode of the SECM operation, where the overall redox process is essentially confined to the thin layer between the tip and the substrate, in SG/TC experiments the tip travels within a thick diffusion layer produced by the large substrate. The system reaches a true steady state if the substrate is a ultramicroelectrode (*e.g.*, a microdisk or a spherical cap) that generates or consumes the species of interest. The concentration of such species can be measured by an ion-selective (potentiometric) microprobe as a function of the tip position. The concentration at any point can be related to that at the source surface. For a microdisk substrate the dimensionless expression is[74,75]

$$c(R,Z)/c(0,L) = \frac{2}{\pi}\tan^{-1}\left[\frac{2}{R^2 + Z^2 - 1 + \sqrt{(R^2+Z^2-1)^2 + 4Z^2}}\right]^{1/2} \quad (13)$$

A somewhat more complicated expression was derived to relate the concentration distribution in the diffusion layer to the flux at the source or sink surface.[29]

One can also evaluate the relative change in the rate of a heterogeneous reaction at the substrate by measuring the concentration of the reaction product at the tip. In this setup, the tip is positioned at a fixed distance from the substrate, and the time dependence of concentration is measured. This simpler approach is based on the proportionality between the heterogeneous reaction rate and the product concentration. It is most useful when the substrate flux cannot be measured directly (*e.g.*, the substrate reaction is not an electrochemical process).[76–78]

Martin and Unwin developed a quantitative treatment for amperometric SG/TC experiments with the separation distance of the same order of magnitude as the tip radius.[33] Although the chronoamperometric current at a macroscopic substrate is time-dependent, the processes in a microscopic gap between the tip and the portion of the substrate surface facing it reaches a quasi-steady state. The concentration profiles of redox species in the gap are similar to those under the positive feedback conditions, and the normalized steady-state collection current-distance data can be calculated from the modified eqn (14)[33]

$$I_c = \frac{i_T}{i_{T,\infty}} = \gamma(0.78377/L + 0.3315\ \exp(-1.0672/L) + 0.68) \quad (14)$$

where γ is the ratio of the diffusion coefficients of the redox species ($\gamma = D_O/D_R$ when solution initially contains the reduced form).

4.2. Numerical solutions of the SECM diffusion problems

The analytical approximations presented above are best fits to numerical simulations of the diffusion problems for relatively simple and well defined electrochemical systems, *e.g.*, an inlaid

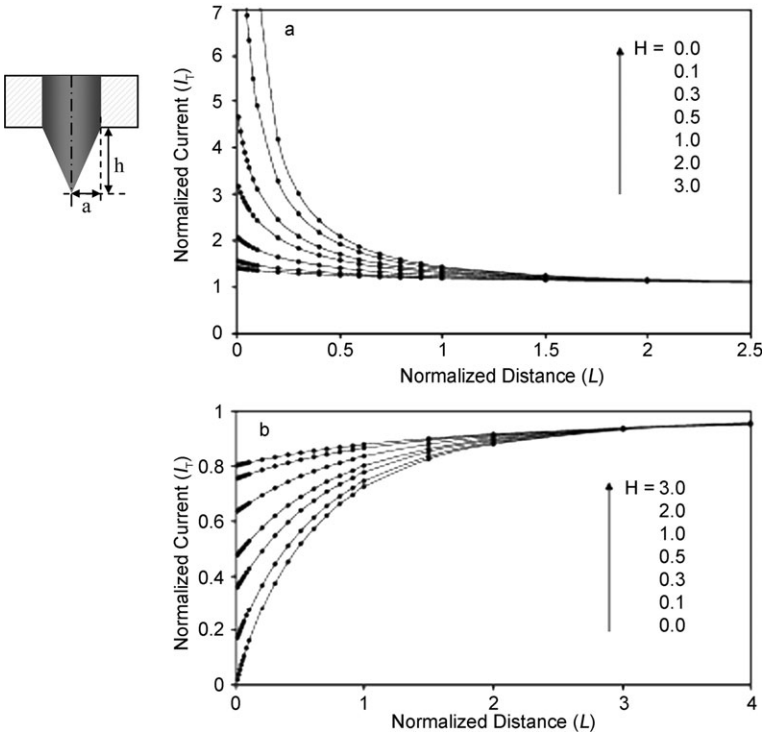

Fig. 7 SECM approach curves for a conical tip geometry (a) positive feedback, (b) negative feedback. H is the ratio of the height to the base radius, $H = h/a$. (Adapted with permission from ref. 14. Copyright 2004, American Chemical Society.)

disk electrode approaching a flat, infinite, and uniformly reactive substrate surface. In most quantitative SECM experiments, the use of such approximations could be justified. However, no analytical approximations are available for more complicated processes and system geometries, and so one has to resort to computer simulations.

4.2.1. Non-disk tip geometries. Although disk-shaped tips are typically most useful for SECM experiments, it is not always possible to produce such tips, especially when they have to be nanometer-sized. For some special applications (*e.g.*, penetration experiments), one may want to purposely fabricate tips with different geometries. To characterize non-disk shaped tips, experimental approach curves are obtained and then compared to simulated ones.[13] A range of UME tip geometries including sphere cups,[15,16] spheres,[17] rings,[18] ring-disks,[19] and etched electrodes[20,34] have been characterized in this way.

A relatively simple technique to produce nanoelectrodes of conical shape is electrochemical etching of partially insulated wires.[14,20] The current-distance curves for a conical electrode approaching either a conductive or an insulating substrate were generated by an approximate procedure[13] and later simulated more accurately.[14,79] Fig. 7 shows the calculated current-distance curves for tips of different conical geometries approaching either a perfect conductor (A) or a perfect insulator (B). It can be seen that the magnitude of either positive or negative feedback decreases with increasing ratio of the cone height to its base radius (H). For $H = 3$, the maximum I_T^C is only $\sim$1.3, and the minimum $I_T^{ins} \cong 0.8$. These working curves can be used to determine the geometry of the electrode for H up to $\sim$3, but because of the dramatically lower feedback at $H > 0.5$, conical tips are not very useful for feedback mode experiments.

Another type of non disk-shaped SECM tips are UMEs shaped as spherical caps. They can be obtained, for example, by reducing mercuric ions on an inlaid Pt disk electrode or simply by dipping a Pt UME into mercury.[16] An approximated procedure developed for conical geometry was also used to model spherical cap tips.[13] Selzer and Mandler performed accurate simulations of hemispherical tips using the alternative direction implicit final difference method to obtain steady-state approach curves and current transients.[15] As with conical electrodes, the feedback magnitude deceases with increasing height of the spherical cap, and it is much lower for a hemispherical tip than for the one shaped as a disk.

4.2.2. Three-dimensional simulations and non-ideal conditions. The above SECM theory was developed by solving two-dimensional axisymmetric diffusion problems. Even for an idealized situation (*i.e.*, a flat, planar substrate, strictly perpendicular to the axis of the well-shaped disk tip) only numerical solutions can be obtained. When deviations from this ideal case occur in a real experiment, one has to evaluate the effects of such deviations and check if the available theory can still be used for data analysis. Similar questions arise when the substrate's topography is complicated and/or its surface reactivity is highly non-uniform.

Fulian *et al.*[80] introduced the boundary element method (BEM)—a powerful numerical method previously employed in engineering computations—for the numerical solution of SECM diffusion problems. The BEM is more suitable for

problems with regions of complex or rapidly changing geometries than the finite difference methods employed in earlier SECM simulations. Fulian *et al*. used the BEM to simulate the current responses for different SECM situations such as a non-disk tip approaching a flat substrate; a flat disk tip over a hemispherical or a spherical cap-shaped substrate or a tilted substrate; a lateral scan of a flat disk tip over an insulating/conductive boundary.

Sklyar and Wittstock[81] used the exterior Laplace formulation combined with the BEM to recalculate the steady-state feedback responses for systems treated in ref. 80. The exterior Laplace formulation assigns no boundaries to the solution therefore it gives a better estimate of the diffusion flux from the bulk solution to the UME. This technique was also applied to numerically simulate other non-axisymmetric experimental situations, such as a lateral scan over a band-shaped substrate. Another simulation addressed the shear-force distance control mode of the SECM. The authors concluded that for an RG of 5.1 a tilt of the probe of up to 8 degrees does not affect significantly the shapes of the i_T-d curves when d is measured from the center of the electroactive area. However, if d is assumed to be the distance between the substrate and the part of the probe closest to it (*i.e*. the glass edge), the shapes of the i_T-d curves changes dramatically, and the attainable maximum positive/negative feedback is much lower. This observation becomes significant when one uses the shear-force mode to control the tip-substrate separation distance because in such experiments the distance is measured between the glass edge and the substrate. Quantitative analysis of SECM data in the shear-force mode is therefore more sensitive to the precision of the tip/substrate alignment.

In a later publication,[82] BEM was used to calculate the steady-state response of an integrated AFM-SECM probe consisting of a non-conducting AFM tip surrounded by the electroactive gold square frame. The feedback current and substrate topography were mapped simultaneously when such a tip was scanned over the substrate. The data from the topographic image (Fig. 8A) were used to calculate the simulated current response. A comparison of the real SECM image and the simulated one (Fig. 8D) shows the accuracy of the simulation and its applicability to the study of systems with complex geometry by SECM. Recently, Sklyar *et al*.[83] developed a method to simulate a diffusion problem involving several diffusing species. To avoid solving complicated diffusion problems involving more than one chemical species, previous experiments were carried out under special conditions or with simplifying assumptions, so that the diffusion of only one redox species needed to be considered. The theory developed in ref. 83 could be useful for experiments with biological cells and other systems in which such simplifications are not appropriate.

5. Applications

5.1. Heterogeneous reactions at solid/liquid interfaces

Heterogeneous ET at the metal/solution interface was the first chemical reaction probed by SECM. Although the diapason of processes studied by this technique has broadened

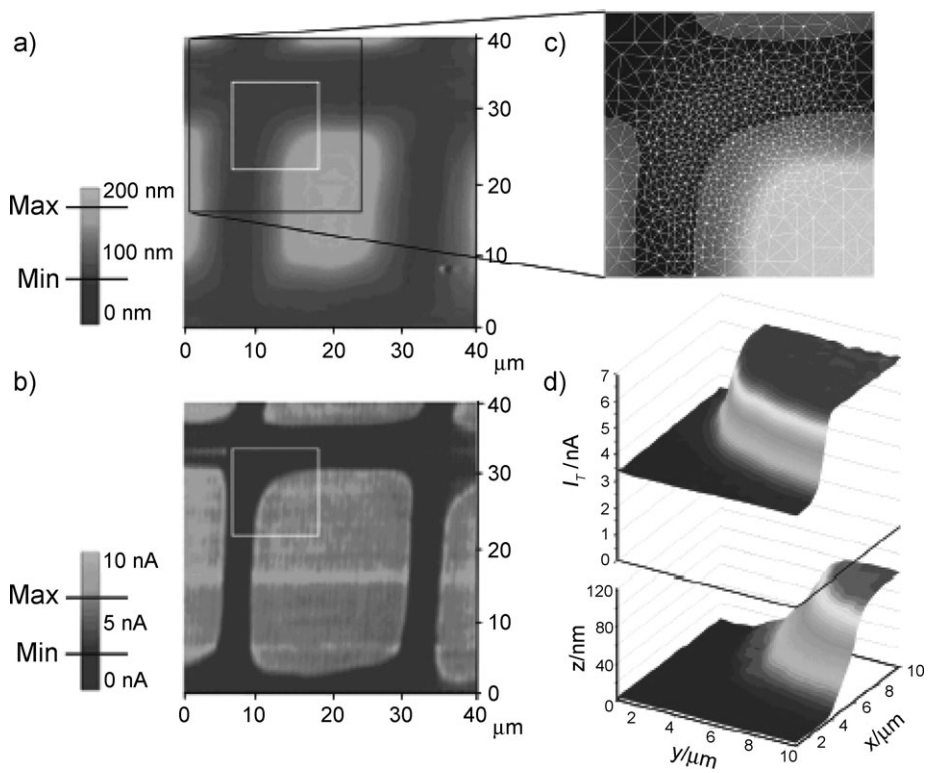

Fig. 8 (a) Experimental AFM contact mode (topography) and (b) SECM feedback images simultaneously obtained with an integrated SECM-AFM probe. (c) Simulation mesh for the area represented by a black rectangle. (d) Simulated SECM feedback current (upper graph) and real topography (lower graph) of the white rectangle area. Solution contained 50 mM $Fe(CN)_6^{4-}$ and 0.5 M KCl. The tip was biased at 600 mV *vs*. Ag QRE. (Reprinted with permission from ref. 82. Copyright 2005, American Chemical Society.)

considerably, heterogeneous processes remain the most popular subject of SECM studies.

5.1.1. Electron transfer kinetics at solid/liquid interfaces. Kinetics of electron transfer is of primary importance for a number of electrochemical systems from fuel cells and batteries to biosensors to solar cells to molecular electronics. To measure the ET kinetics under steady-state conditions, the mass transfer rate has to be sufficiently high, and the uncompensated resistive potential drop in solution (*IR*-drop) must be small enough so as not to affect the results. The feedback mode of SECM meets these two requirements allowing one to study fast ET reactions.

The SECM can be used to measure heterogeneous ET kinetics either at the tip or at the substrate electrode. In both cases, the effective mass-transfer coefficient can be expressed by eqn (12), and a high mass-transfer rate can be achieved under steady-state conditions by decreasing the tip-substrate separation distance. The ET kinetics at the tip can be determined from steady-state voltammetry. The substrate is kept at a constant potential, such that the ET reaction at its surface is diffusion-controlled, while the tip potential is swept slowly to record a voltammogram. The ET rates, which are too fast to be measured when the tip is far from the substrate, can be determined at sufficiently small d. In this way several fast rate constants ($k^\circ > 1$ cm/s) were measured with micrometer-sized SECM tips.[84–86]

Recently, nanometer-sized electrodes were employed to measure the kinetics of several fast ET reactions by this method.[54] The disk-type, polished Pt nanoelectrodes (3- to 400-nm radius) were characterized by combination of voltammetry, scanning electron microscopy, and SECM. A number of voltammograms were obtained at the same nanoelectrode to attain the accuracy and reproducibility similar to those reported previously for micrometer-sized probes. In this way, the self-consistent kinetic parameter values with the uncertainty margin of $\sim$10% were obtained for electrodes of different radii and for a wide range of the SECM tip/substrate separation distances. Fig. 9 shows voltammograms of 1 mM ferrocenemethanol obtained at different separation distances between the 36-nm-radius polished Pt tip and the evaporated gold substrate. The kinetic parameters (k°, α) and the formal potential of the ET reaction were extracted by fitting experimental voltammograms to the theoretical curves calculated from eqn (10). In this way, the kinetic parameters were obtained for several rapid ET reactions, of which the fastest was $Ru(NH_3)_6^{3+}$ reduction in KCl ($k^\circ = 17.0 \pm 0.9$ cm/s).

To probe heterogeneous electron transfer kinetics at the substrate surface, the tip is held at a potential where the ET reaction is diffusion controlled, and the approach curves are recorded for different substrate potentials.[87] In case of irreversible ET, the rate constant can be extracted by fitting the experimental approach curve to eqn (11). No analytical theory exists for quasi-reversible substrate ET, and measuring such kinetics is not straightforward.[63]

The above approach was later extended to investigate more complicated systems involving multistep processes and parallel reaction pathways. For example, in a study of ET at self-assembled monolayers (SAMs), the SECM was used to measure independently the rates of ET mediated by monolayer-attached redox moieties and direct ET through the film, as well as the rate of the bimolecular ET reaction between the attached and dissolved redox species.[69a] SAMs were assembled onto evaporated gold electrodes from solution containing a mixture of *n*-alkylthiol and ferrocenyl-alkanethiol. Several different situations were considered (Fig. 10): the monolayer either contained attached redox centers (Fig. 10A) or simply acted as a blocking layer (Fig. 10B). In the former case, ET occurred *via* a bimolecular reaction between dissolved redox species generated at the tip (R) and redox centers attached to the SAM (M^+), which was followed by electron tunneling. In Fig. 10B, ET occurred *via* direct tunneling between the dissolved species, R, and the electrode. Finally, the charge transfer could occur through pinhole defects in the film (Fig. 10C). The possibility of measuring the rates of all of these processes and analyzing the combinations of different competing pathways for the long-distance ET was demonstrated. The upper limits for the electron tunneling and bimolecular rate constants measurable by the developed technique were given as $\sim 10^8$ s^{-1} and $\sim 5 \times 10^{11}$ mol^{-1} cm^3 s^{-1}, respectively, assuming the use of a micrometer-sized tip.

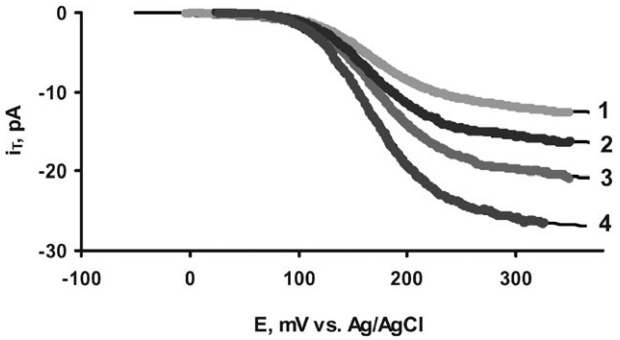

Fig. 9 Experimental (symbols) and theoretical (sold lines) steady-state voltammograms of 1 mM ferrocenemethanol obtained at different separation distances between the 36-nm Pt tip and Au substrate. $d = \infty$ (1), 54 nm (2), 29 nm (3), and 18 nm (4). $v = 50$ mV/s. Theoretical curves were calculated from eqn (10). (Adapted with permission from ref. 54. Copyright 2006, American Chemical Society.)

5.1.2. Electrocatalysis. The capability of SECM to detect and to image regions with different catalytic activities has been exploited by several groups.[88–91] So far, the SECM has mostly been used to study two electrocatalytic reactions, the hydrogen oxidation reaction (HOR) and the oxygen reduction reaction (ORR), because of their importance for fuel cells and other applications.

$$H_2 - 2e^- \rightarrow 2H^+ \quad \text{(HOR)} \qquad (15a)$$

$$O_2 + 2H_2O + 4e^- \rightarrow 4OH^- \quad \text{(ORR)} \qquad (15b)$$

Unlike typical redox mediators used in SECM, which exhibit fast, reversible ET at any conductive surface, the rates of oxygen and hydrogen reactions strongly depend on the catalytic activity of the substrate surface.

Kucernak *et al.* studied the hydrogen evolution reaction on the platinum black electrocatalyst dispersed onto a flat highly

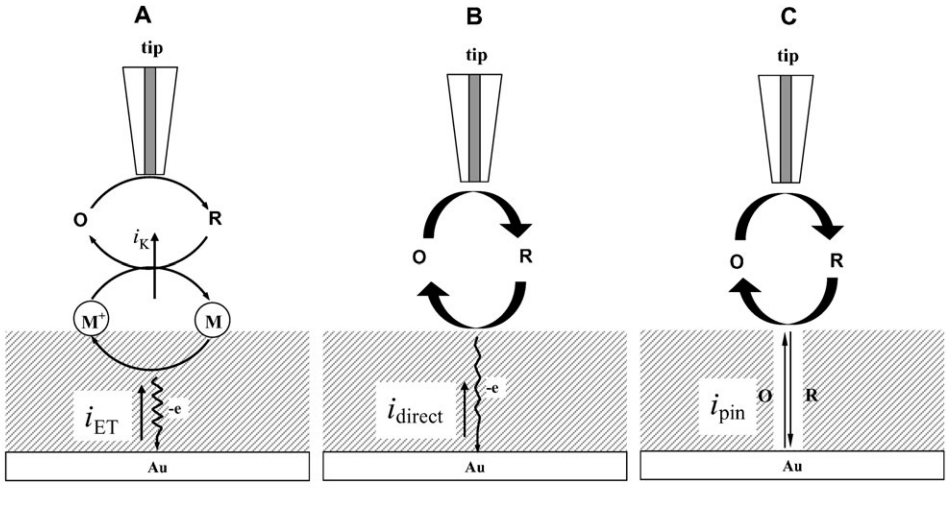

Fig. 10 Schematic view of the processes involved in the SECM measurements of ET across an electroactive SAM. (A) Mediated ET; (B) direct electron tunneling through monolayer; and (C) ET through pinholes. (Reprinted with permission from ref. 69a. Copyright 2004, American Chemical Society.)

oriented pyrolytic graphite (HOPG) electrode.[92] The activity of individual catalyst particles as a function of substrate potential was studied. The tip was also rastered over the HOPG/Pt substrate to produce images that reflect the local molecular hydrogen concentration and, thus, the local rate of hydrogen evolution. Zhou *et al.*[89] studied proton reduction from a 0.01 M $HClO_4$ solution at different substrates (Pt, Au) by feedback mode of the SECM. The HOR rate was determined quantitatively at different substrate potentials from SECM approach curves. These authors also studied the effect of the surface oxide and anion adsorption on hydrogen oxidation.

ORR cannot be studied by feedback mode in neutral or acidic buffers. The tip-generated ORR product, *i.e.* hydroxide ion, immediately reacts with aqueous hydrogen ions to form water and doesn't have time to diffuse toward the substrate. A similar situation is encountered when the HOR is probed in neutral or alkaline media. Fernández *et al.*[93] employed the TG/SC mode to study the ORR on the substrate in acidic solutions. The tip is placed close to the substrate and biased at a potential at which water is oxidized to oxygen. The substrate potential is fixed at a value corresponding to oxygen reduction to water. The oxygen reduction rate at the substrate surface reflects its electrocatalytic activity.

By combining TG/SC mode with surface scanning capability, one can screen several metals or mixtures of metals for their electrocatalytic activities. Combinatorial screening methods are widely used to search for novel metallic electrocatalysts.[94] For rapid screening SECM experiments, arrays of bimetallic or trimetallic catalyst spots with different compositions were produced.[95] Each spot contained some binary or ternary combination of Pd, Au, Ag, and Co deposited on a glassy carbon substrate (Fig. 11A). The electrocatalytic activity of these materials for the ORR in acidic media (0.5 M H_2SO_4) was examined using SECM in a rapid-imaging mode. The SECM tip was scanned in the *x*-*y* plane over the substrate surface while electrogenerating O_2 from H_2O at constant current. By scanning at step intervals of 50 μm every 0.2 s, the area as large as 7×7 mm^2 could be screened in about 5 h. Thus, one could rapidly screen arrays covering a wide range of catalyst compositions for their activity toward the ORR, and the combinations of metals with enhanced electrocatalytic activities could be identified (Fig. 11B and C). The authors also compared the activity determined by classical rotating disk electrode (RDE) and the SECM screening technique and found that the activity of catalyst spots evaluated by SECM agrees with that of the carbon black supported catalyst mixtures on a GC RDE. In this way, Fernández *et al.* proposed the guidelines for the design of improved bimetallic electrocatalysts for ORR in acidic media. Later,[96] the same group found two new catalysts, Pd–Co–Au (70:20:10 atom %) and Pd–Ti (50:50 atom %), that show essentially equal or slightly better performance than the more expensive Pt catalysts currently used for the ORR in PEMFC.

In another combinatorial study, Weng *et al.* used poly (L-histidine) (poly-his) as a matrix and ligand to complex Cu^{2+} and mimic the active sites of oxygen reductases.[97] The electrocatalytic activity for oxygen reduction was evaluated on an array of Cu^{2+}-poly-his spots of different compositions deposited on a glassy carbon electrode. The highest efficiency and stability of the complex for oxygen reduction reaction was found at a Cu^{2+} mole fraction in the range of 0.17–0.35. Although the electrocatalytic activity of this complex is still lower than that of laccase, the authors suggested that different polypeptides and their mixtures and different preparation conditions may yield better results.

In an effort to discover and characterize new catalyst formulations for HOR, Hillier *et al.*[98] deposited a layer of Pt with a coverage gradient on a catalytically inactive indium-tin oxide substrate. The reactivity gradient of this catalyst was measured directly as a function of spatial position using a SECM in the feedback mode. It was found that the nonuniform platinum coverage generates a variation in the hydrogen oxidation rate constant. The local reaction rate was

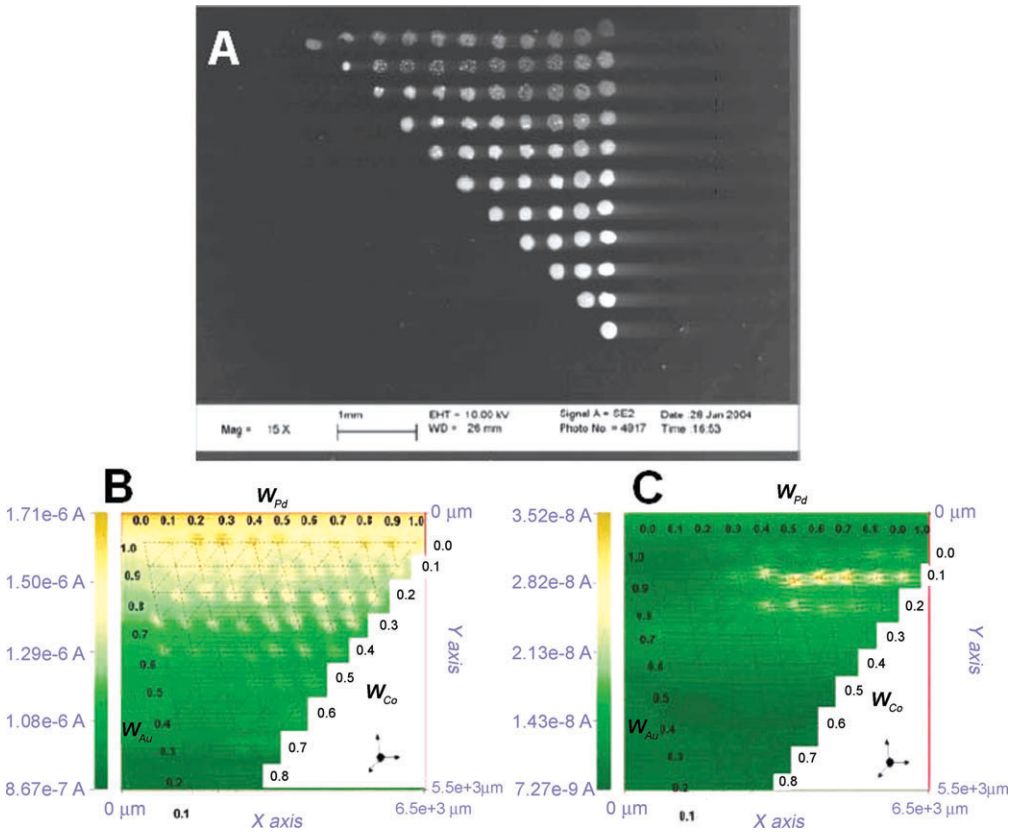

Fig. 11 (A) SEM image of typical ternary catalyst Pd–Au–Co array. (B, C) SECM-TG-SC images of oxygen reduction activity on Pd–Au–Co arrays in 0.5 m H_2SO_4 with substrate biased at 200 mV (B) and 750 mV (C) *vs.* hydrogen reference electrode. Tip substrate distance was 30 µm, tip current was −160 nA, and scan rate was 50 µm each 0.2 s. W_M is the atomic ratio of metal M in the spot. (Reprinted with permission from ref. 95. Copyrights 2005, American Chemical Society.)

proportional to the local platinum surface coverage, as determined by electron microscopy. In another report from the same group,[99] the activity of Pt_xRu_y and $Pt_xRu_yMo_z$ catalysts for oxidation of hydrogen was studied as a function of composition and electrode potential.

5.2. Lateral mass/charge transfer

A promising application of SECM is to the measurement of lateral charge and mass transfers. Unwin group[100] studied the lateral mass transfer of a surfactant at the air/water (A/W) interface. The electroactive surfactant, N-octadecylferrocenecarboxamide ($C_{18}Fc^0$) was mixed with 1-octadecanol in a 1 : 1 ratio and spread onto water to form a Langmuir monolayer. A 25 µm diameter submarine tip (*i.e.*, a Pt UME sealed in a U-shaped glass capillary with the conductive surface pointing upward) was placed 1 to 2 µm away from the A/W interface. The first "bleaching" period involved stepping the tip potential to a value at which $Ru(bipy)_3^{2+}$ (the form initially present in the solution) was oxidized to $Ru(bipy)_3^{3+}$. The oxidant diffused toward the A/W interface and reacted with $C_{18}Fc^0$ thus effectively "bleaching" the monolayer locally. During the second period, the potential step was reversed to convert the electrogenerated species to its initial form. This allowed the monolayer to recover by 2D diffusion of $C_{18}Fc^0$ and $C_{18}Fc^+$ in/out of the bleached area. The third potential step was in the same direction as for the first one. The shape of the corresponding tip current-time transient depends strongly on the duration of the second period, which in turn determines of surface diffusion of $C_{18}Fc^0$. This dependence was used to determine the lateral diffusion coefficient of the amphiphile. The rate constant of ET between the solution mediator and the surface-confined species was also determined from the current-time transients. A computer simulation was used to fit the data, and the values of $D_{surf} = 1.0 \pm 0.2 \times 10^{-6}$ cm^2 s^{-1} and $k = 0.035$ cm s^{-1} were found for a surface coverage of $\Gamma = 1.66 \times 10^{-10}$ mol cm^{-2}.

In a later publication,[101] Unwin group studied the lateral charge propagation in $Os(bpy)_2(PVP)_nCl]Cl$ thin films with $n = 5$ and 10. The UME tip was positioned about one radius away from the spin-coated metallopolymer. A three-step experiment similar to those described in ref. 100 was conducted using $Ru(CN)_6^{4-}$ as a redox mediator. In the first step, the Os(II) moieties of the metallopolymer were oxidized to Os(III). During the second step, the concentration of Os(II) under the tip was recovered by electron hopping in the monolayer (*via* self-exchange reaction between Os(III) and Os(II) moieties). The rate of the lateral charge transport was determined by fitting the current-time transients obtained in the third, final step to theoretical curves generated using FEMLAB simulation package. The effective diffusion coefficient for the electron hopping as low as 10^{-10} cm^2 s^{-1} could be measured. The rate of the ET between $Ru(CN)_6^{3-}$ and Os(II)

at the film/solution interface was diffusion limited. The same group has also developed a method to determine the conductivity of ultra-thin films using SECM under steady-state conditions, *i.e.*, from the current-distance curves.[102] They demonstrated the usefulness of their approach by investigating the effect of surface pressure on conductivity of a polyaniline monolayer at the water/air interface.

5.3. SECM/AFM and other hybrid techniques

The combination of spatially resolved electrochemical experiments with different types of measurements made at the same time and (if possible) at the same location is a powerful approach to studies of surface structures and dynamics. A number of analytical techniques have been combined with SECM including near-field scanning optical microscopy (NSOM), surface plasmon resonance (SPR), electrochemical quartz crystal microbalance (EQCM), fluorescence spectroscopy (FS), electrogenerated chemiluminescence (ECL), and atomic force microscopy (AFM). The corresponding hyphenated methods are NSOM-SECM,[103] EQCM-SECM,[104–106] SPR-SECM,[107] FS-SECM,[108] ECL-SECM,[109] and AFM-SECM.[110]

Among these hybrid methods, AFM-SECM is most widely used. One of the strength of the AFM-SECM technique is in its positioning capabilities. Using the AFM mode, one can position a submicrometer-sized tip near the substrate surface and keep a constant tip-substrate distance during the surface raster. Maintaining a constant distance between the tip and the substrate is essential for avoiding tip crashes and the damage to sample during the imaging of a substrate with non-uniform surface reactivity and/or complex topography.

Several groups employing SECM-AFM technique have developed different approaches to the tip fabrication.[20,111–113] These included hand-fabricated probes, made from an etched, insulated wire with the exposed end;[20,111,112] AFM tips with a frame electrode fabricated by coating a commercial silicon nitride probe with a metal and an insulator and using focused ion beam technology to reshape the probe and expose the tip;[113,114] nanoelectrode probes based on the use of single-walled carbon nanotube bundles on AFM tips;[115,116] and batch microfabricated probes.[117,118] The batch microfabrication was carried out on silicon wafers, yielding 60 probes in each run. The process yields sharp AFM tips, incorporating a triangular-shaped electrode at the apex. Fig. 12 shows two different kinds of SECM-AFM probes. The first type (Fig. 12A), called conducting-AFM probe (C-AFM), can be used to acquire information about the electrochemical activity of a non-conductive substrate with electroactive species attached to its surface (*e.g.* oxidoreductase adsorbed on a glass slide). The probe in Fig. 12B is suitable for conductive substrates: the insulation of the AFM tip prevents direct electrical contact between its conductive core and the substrate. Studies of non-conductive crystal dissolution have been done with C-AFM probes.[119] The probe was first used amperometrically to induce crystal dissolution and the resulting changes in topography were imaged in the AFM regime. Other applications like nanoscale imaging of the electronic conductivity of oxide films on Ti,[120] probing diffusion through single nanoscale

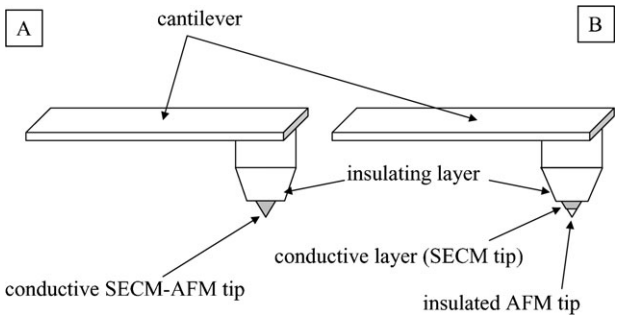

Fig. 12 (A) Conducting and (B) non-conducting SECM-AFM tips. (A) The SECM and AFM tips are made from the same conducting material; (B) the AFM tip is insulated to prevent direct electrical contact with the conductive substrate surface.

pores,[121] the studies of electrochemical properties of a boron-doped diamond electrode[122] and a $Ti/TiO_2/Pt$ electrode,[123] have made use of C-AFM tips.

When the tip is scanned laterally above the substrate, the obtained image reflects both the surface topography and the distribution of its chemical reactivity. This makes the data interpretation difficult if no *a priori* information on the substrate topography is available. One way to avoid this problem is to maintain a constant tip-substrate distance during the raster of the substrate surface. The AFM-SECM mode achieves this by controlling the tip substrate distance with the AFM sensor. Thus, a raster in the AFM-SECM mode simultaneously produces a surface topographical map and a surface reactivity map (see, for example, Fig. 8A and B). This makes the SECM-AFM combination very useful for imaging substrates of complex topography and variable reactivity. Davoodi *et al.* used AFM-SECM to study the corrosion of Al in NaCl solution.[124] The complimentary topographical and electrochemical activity maps have been obtained of the same surface area with the micrometer lateral resolution. Kranz *et al.*[125] integrated a submicrometer-size electrode into an AFM tip at the exactly defined distance from the apex using focused ions beam technology. They used such probes to study micropatterned samples with immobilized enzyme spots. The AFM contact mode provided the topography of the sample. Since the SECM can be used to study the enzyme activity in generation/collection mode, AFM-SECM could simultaneously probe the topography of the enzyme pattern and its local activity. A somewhat similar approach was also used in ref. 126.

Other recent applications of AFM-SECM included the study of the iontophoretic transport of $Fe(CN)_6^{4-}$ across a synthetic track-etched polyethylene terephthalate membrane by Gardner *et al.*[127] They made the structure and flux measurements at the single pore level and found that only a fraction of candidate pore sites are active in transport. Demaille *et al.* used AFM-SECM technique in aqueous solutions to determine both the static and dynamical properties of nanometer-thick monolayers of poly(ethylene glycol) (PEG) chains end-grafted to a gold substrate surface.[113]

The development of comprehensive theory for SECM-AFM method is challenging because of complicated geometries of

the employed tips. Holder *et al.*[128] reported quantitative modeling of mass transport at metal-coated AFM probes that can be used for flux-generation in SECM-AFM experiments. The theory was also developed for a frame electrode integrated with an AFM probe.[82,129]

5.4. Surface patterning and modification

The SECM can be used to fabricate microstructures on surfaces by deposition of metals or other solids or by etching the substrate (micropatterning of substrates with enzymes will be discussed in section 5.5.2). The two main approaches have been used, the direct mode[130] and the feedback mode.[131]

In a typical direct mode experiment, the tip is held in a close proximity to the substrate, and the voltage is applied between them to cause the desired reaction at the substrate. Direct deposition of metal lines on polymer-coated substrates was reported by Bard group in the late 1980s.[130,132,133] A similar approach has been used to deposit polyaniline on a Pt substrate covered with a Nafion film loaded with anilinium ions.[134] The substrate was biased at a positive potential to electropolymerize aniline just under the tip which, acting as a cathode, reduced protons to hydrogen. Forouzan and Bard[135] used the thin (10–15 Å) water layer that condenses on a mica substrate in humid atmosphere for direct mode deposition of silver.

Direct etching of a metal substrate (*e.g.*, Cu) covered with a Nafion film was accomplished by biasing the substrate at a positive potential with respect to the tip.[132] In this case, a mediator such as MV^{2+} was introduced into the film and reduced at the tip. The etching resolution attainable by this technique is lower than that for the deposition at the tip because the electric field distribution yields a lower current density at the substrate than at the tip. The resolution attainable in direct deposition and etching depends on a number of factors: the tip size, the penetration depth, the tip current, and scan rate. The faster scan rates tend to yield smaller features. However, fast scanning across the surface produces a higher contribution from charging current. Typical maximum scan speeds applied are about 500 nm/s. Instrumental factors, *e.g.*, vibration-damping, feedback response, and temperature control, are also important for high-resolution experiments, as are the reactions at the tip and substrate.

In the feedback mode surface patterning, a redox mediator is present in the solution. The tip-generated redox species must be able to induce the desired reaction (*i.e.*, deposition or etching) at the substrate and be regenerated at its surface. For example, a strong oxidant, like Br_2, generated at the tip by oxidation of Br^- can etch the area of the substrate, *e.g.* GaAs, directly under the tip.[136] Clearly, a small tip size and close tip-substrate spacing are required for high resolution. The regeneration of the mediator at the substrate yields positive feedback current. Thus, the usual approach curves can be employed to estimate the tip-substrate separation distance.

In the feedback mode metal deposition, the tip-generated species reacts with a thin film of metal precursor on the substrate surface.[137] For example, Au or Pd were electrodeposited in PVP films containing $AuCl_4^-$ or $PdCl_4^{2-}$ by generating a suitable reductant (*e.g.*, $Ru(NH_3)_6^{2+}$) at the tip. Shohat and Mandler[138] developed a method to "focus" the diffusion field of the reductant under the tip in order to narrow the region of metal deposition. $Ag(NH_3)_2^+$ served as metal precursor, and the gold substrate was biased at a moderate negative potential, so that aqueous Ag^+ could be reduced but not $Ag(NH_3)_2^+$. The tip generated protons by oxidizing nitrite (reaction 16a), and the increased local acidity shifted the dissociation equilibrium of the diamminesilver complex (reaction 16b) to the right. Silver ions generated by the latter reaction were reduced at the substrate (reaction 16c):

$$NO_2^- + H_2O \rightarrow NO_3^- + 2H^+ + 2e^- \quad \text{(tip)} \qquad (16a)$$

$$\underset{\text{(tip/substrate gap)}}{Ag(NH_3)_2^+ + 2H^+ \rightarrow Ag^+ + 2NH_4^+} \qquad (16b)$$

$$Ag^+ + e^- \rightarrow Ag \text{ (substrate)} \qquad (16c)$$

The addition of ammonia to the solution made the silver pattern narrower by complexing aqueous silver immediately outside the reaction zone. This effect was given the name of "chemical lens".

One of the advantages of the feedback mode deposition is that the substrate needs not be a conductor. Heinze and coworkers used the above method for the deposition of silver lines on both conducting substrate[139] and on a smooth Teflon surface.[140] Benzoquinone served as mediator and the AgCl film was "chemically developed" during the SECM scanning by local reduction of surface Ag^+ ions with electrogenerated dihydroquinone. The small metallic silver clusters formed on the surface of the AgCl film were grown further by "physical development" of the photographic process, in which the reduction of Ag^+ ions and the oxidation of dihydroquinone occurred at different locations on a metallic silver cluster.

Recently, Neufeld *et al.*[141] used SECM to modify a TCNQ substrate to obtain a pattern of the semiconductor CuTCNQ phase (phase I). In their experiment, phase I was formed by using the tip-generated V^{2+} to reduce TCNQ in the presence of Cu^{2+} at the solid-liquid interface (Fig. 13). The possible mechanism of the formation of crystals is:

$$V^{3+}_{(aq)} \rightarrow V^{2+}_{(aq)} \quad \text{(tip)} \qquad (17a)$$

$$\underset{\text{(substrate)}}{\begin{aligned} V^{3+}_{(aq)} &\rightarrow Cu^{2+}_{(aq)} + TCNQ \\ &\rightarrow V^{3+}_{(aq)} + [Cu^{2+}_{(aq)}TCNQ^{\bullet -}]^+_{(transient)} \end{aligned}} \qquad (17b)$$

$$\underset{\text{(substrate)}}{\begin{aligned} [Cu^{2+}_{(aq)}TCNQ^{\bullet -}]^+_{(transient)} + V^{2+}_{(aq)} \\ \rightarrow V^{3+}_{(aq)} + Cu\ ^+TCNQ^{\bullet -}_{(s)} \end{aligned}} \qquad (17c)$$

Fig. 13A shows the initial formation of CuTCNQ. In the growth process of the CuTCNQ phase (step 2), the oxidation of V^{2+} and the reduction of TCNQ and Cu^{2+} do not take place at the same location (Fig. 13B and C).

Mandler's group developed a new method for micropatterning.[142a] They used a micropipette to locally generate ions by potential-assisted ion transfer across the liquid–liquid

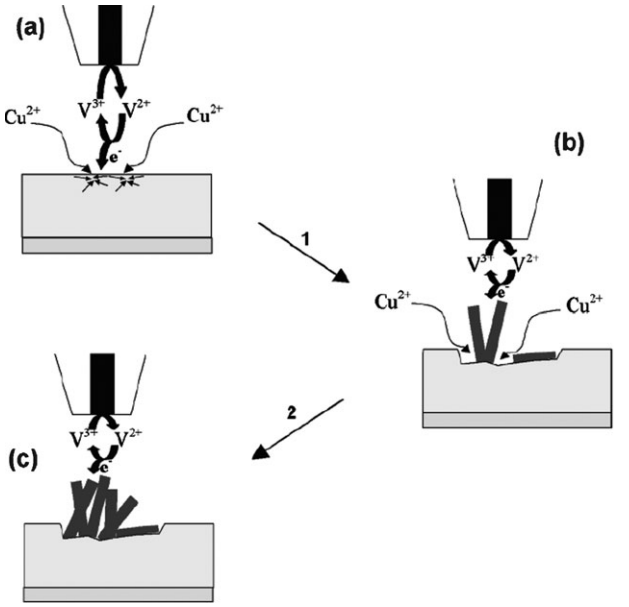

Fig. 13 Schematic diagram illustrating the formation of CuTCNQ by SECM. The CuTCNQ crystals are not drawn to scale. (Reprinted with permission from ref. 141. Copyright 2005, American Chemical Society.)

interface. A micropipette filled with an aqueous solution containing Ag^+ ions was immersed in an organic solution thus creating the ITIES (*cf.* section 2.5). By adding dibenzo-24-crown-8 (DB24C8) to organic phase, a positive feedback could be observed when the micropipette was brought close to a gold slide. DB24C8 diffused toward the micro-ITIES and formed a complex with silver ions. The product of that reaction, Ag^+(DB24C8), was transferred to organic phase, diffused toward the gold surface, and was reduced to silver thus releasing DB24C8. Later,[142b] the same group modified this method to improve the resolution of metal deposition.

Etching can be carried out in the feedback mode by generating an appropriate oxidant (etchant).[130] For example, Cu was etched by $Os(bpy)_3^{3+}$ generated at the tip

$$Cu + 2Os\ (bpy)_3^{3+} \rightarrow Cu^{2+} + 2Os\ (bpy)_3^{2+} \qquad (18)$$

The tip was held at a positive potential, so there was no tendency to plate Cu on the tip, which could be a problem for direct mode etching. Moreover, since the substrate was maintained at a more negative potential, no copper oxidation occurred far from the tip.

An *in situ* formation of conductive domains by electroreduction and local metallization of polytetrafluoroethylene (PTFE) was discussed in a series of reports by Combellas *et al.*[143] The authors carried out both steady-state and transient SECM experiments to investigate the kinetics of PTFE carbonization and concluded that the propagation of the conductive PTFE zone is governed by an in-depth diffusive process.

5.5. Biological systems

Several SECM-based approaches have been developed to study charge transfer reactions in biological systems, including immobilized enzymes and whole cells. The SECM can also be used to image topography and reactivity of biological specimen.

5.5.1. Experiments with living cells. Two main types of SECM experiments on living cells are generation/collection measurements (Fig. 14A and B) and feedback-mode amperometric experiments (Fig. 14C and D). The former approach involves tip positioning in the proximity of a field of immobilized cells (or a relatively large individual cell), with a separation distance sufficiently long for the SECM feedback to be negligible. The tip in this case is used as a passive probe to monitor the concentrations and/or fluxes of redox species generated (or consumed) by the cells. In contrast, the tip/cell separation distance in a feedback mode experiment is sufficiently small to observe either positive or negative feedback from a single immobilized cell. The tip is used to oxidize (or reduce) a redox mediator, and a cell acts as a substrate whose topography and redox reactivity can be probed, as discussed in the previous sections.

5.5.1.1. Monitoring respiration and other cellular functions. Tip collection mode of SECM has been extensively used to study respiration and photosynthetic activities of individual biological cells. Bard and coworkers focused on plant cells.[144] They studied the bottom surface of a *Ligustrum sinensis* leaf and found several stomata structures, which are involved in photosynthesis. Tsionsky *et al.*[145] used the SECM to study the leaves of a plant, *T. fluminensis*. They imaged the topography and probed photoelectrochemistry of single guard cells. In the dark, the stomatal pores surrounded by guard cells were opened by applying KCl solution so that high resolution topographic images could be obtained in the negative feedback

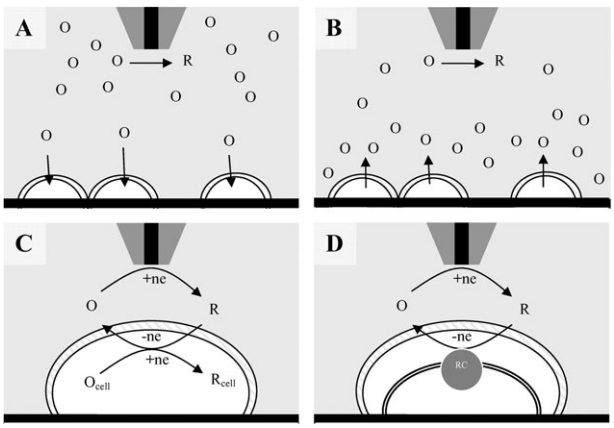

Fig. 14 Schematic diagrams of the SECM experiments with cellular organisms. (A, B) In the SG/TC mode, the tip is used to measure the cellular activity that results either in consumption (A) or production (B) of redox species, O. (C) Bimolecular ET between hydrophobic redox mediator (O/R) and intracellular redox species (O_{cell}/R_{cell}). (D) ET between redox mediator (O/R) and redox center (RC) inside a prokaryotic cell (*e.g.*, of *Rb. Sphaeroides*).

mode with O_2 mediator. Ding's group[145] studied oxygen evolution above single stomata in *Brassica juncea in vivo*. After the plant was treated with 0.2 mM $CdCl_2$, they found the stomatal density to be lower, and the stoma size to increase. They also found that oxygen evolution above individual stomatal complexes in Cd^{2+} treated plants was slower than that from control plants. Holt and Bard[146] studied the antimicrobial effect of micromolar concentration of $AgNO_3$ on *E. coli*. by SECM. They found the rate of respiration increased initially on the addition of $AgNO_3$, followed by cessation of respiration.

Matsue and co-workers used the SECM to monitor respiration activities in a wide variety of living individual cells. They mapped oxygen fluxes at the cell surface associated with respiration and photosynthesis.[147] By measuring the rate of oxygen consumption, the authors addressed a number of biomedical problems from drug sensitivity of cancer cells[148] to viability of a bovine embryos[149] to mitochondrial respiration in neuronal cells.[150]

5.4.1.2. Cellular redox processes. Liu *et al.* applied the SECM feedback mode to non-invasively probe the redox activity of individual mammalian cells.[70,71] In order to probe the redox activity of mammalian cell, both oxidized and reduced forms of the redox mediator must be capable of crossing the cell membrane and shuttling the charge between the tip electrode and the intracellular redox centers (Fig. 14C). Only hydrophobic redox mediators (*e.g.*, menadione and 1,2-naphthoquinone) could be used in SECM experiments with mammalian cells.[71] The tip and intracellular redox reactions can be presented as follows:

$$O + ne = R \quad \text{(at the tip electrode)} \tag{19a}$$

$$R + O_{cell} \xrightarrow{k} O + R_{cell} \text{(inside the cell)} \tag{19b}$$

The i_T *vs.* d curves were obtained by moving the tip (negatively biased, so that reaction 19a is diffusion controlled) toward the cell membrane and fitted to the theory to extract the value of the effective heterogeneous rate constant (k). Reaction 19b is a complicated process involving at least three steps: (i) generation of redox centers (O_{cell}) inside the cell, (ii) transport of mediator species across the cell membrane, and (iii) bimolecular ET between the mediator species and intracellular redox centers. Mechanistic analysis showed that, depending on the properties of the mediator (*e.g.*, formal potential, ionic charge, and hydrophobicity), the main factor limiting the overall charge transfer rate can be either the membrane transport, or the availability of intracellular redox agents, or the driving force for the ET reaction, *i.e.*, the difference between the intracellular redox potential and the formal potential of the mediator.[71] Kinetic parameters were determined for different steps of the charge-transfer process.

Using this approach, significant differences were detected in the redox responses given by three types of human breast cells with different levels of protein kinase Cα (PKCα, an enzyme that has been linked with motility and metastasis of various cell types); non-metastatic MCF-10A cell (a human breast epithelial cell), 11α cell (a breast cell with engineered overexpression of PKCα), and MDA-MB-231 (a highly metastatic breast cancer cell expressing a high level of PKCα). Approach curves obtained with these cells and several redox mediators demonstrated that their cellular redox activities are in the order of MCF-10A > 11α > MDA-MB-231. This result indicated that metastatic human breast cells can be electrochemically distinguished from non-transformed breast cells. The obtained kinetic data were used to identify the experimental conditions, such as the nature and concentration of the redox mediator, which would maximize the detection of metastatic cells in a field of normal breast cells and in tissue samples.[73]

Purple bacteria (*Rb. sphaeroides*) were also investigated by SECM.[72,151] Unlike mammalian cells, *Rb. Spheroides* have two membranes (outer and cytoplasmic) and no nucleus (Fig. 14D). The outer membrane is permeable to both hydrophilic and hydrophobic redox species while the cytoplasmic membrane is impermeable to hydrophilic redox species and contains redox centers. Because of this difference, ET processes in *Rb. sphaeroides* were probed using both hydrophobic and hydrophilic (*e.g.*, $Fe(CN)_6^{3-/4-}$) redox couples. Cai *et al.*[72] found that the effective rate constant of the redox reaction of hydrophilic mediators (*e.g.* different quinones) with intracellular redox centers correlates with the mediator formal potential and estimated cytoplasmic and periplasmic redox potentials. Longobardi *et al.*[151] used chromatophores (specialized pigment-bearing structure obtained from the mechanical rupture of the *Rb. Sphaeroides*) and liposomes (reconstituted membrane systems) in order to investigate solely the role played by the cytoplasmic membrane of the bacterium. They found that the SECM feedback process is mediated by membrane-bound redox species (Fig. 14D) and that the oxidant species inside *Rb. Sphaeroides* is most probably the ubiquinone that resides in the cytoplasmic membrane pool.

The above methods for cell investigation are essentially non-invasive. However, to localize the redox activity in different cell compartments (*e.g.*, mitochondria) the tip must penetrate the cell. The most recent effort focused on using nanometer-sized tips and nanopipette-based probes for high-resolution studies of mammalian cells.[38] It was shown that amperometric nanoprobes allow quantitative spatially resolved SECM measurements inside living cells. The use of a tip ~1000 smaller than the cell greatly minimizes the damage to the cell membrane and may facilitate sub-cellular level studies of biologically relevant charge-transfer processes.

5.5.1.3. Imaging living cells. Most SECM images of living cells were obtained in a constant-height mode, where the tip is rastered in a horizontal (x-y) plane above the substrate surface. Using this approach, one can map the fluxes of oxygen and other redox species,[147] image the cell topography under either positive or negative feedback conditions,[144,152] and also map its redox reactivity.[70] Baur and co-workers imaged topography of single PC12 neuron cells using a constant-height mode based on the negative SECM feedback.[153] In this study, PC12 cells before and after exposure to nerve growth factor (NGF) were imaged using $Ru(NH_3)_6^{3+/2+}$ mediator. Because the cell membrane was impermeable to the redox species, it acted as an insulating substrate in topographic imaging experiments. The constant height mode was

also used in combination with fluorescence microscopy to image fields of different types of human breast cells in monolayer culture.[73]

A serious problem with constant-height imaging of living cells arises from significant variations in height between different parts of such a cell.[153] This problem is even more important in multi-cell imaging because different cells (and especially species of different types) are different with respect to their size and shape.[73] Since some cells are taller than others, it is not easy to image a heterogeneous field of cells without scratching any of them. If the tip radius is smaller than the difference between the heights of two cells in the field (or the heights of different parts of the same cell), either the taller cells are scratched in the process of constant-height imaging, or the lower cells are not imaged clearly. One way to obviate this difficulty is to use a relatively large tip and to scan it within 1-2 tip radii above the cell surface. However, the use of a larger tip decreases spatial resolution.

The above problems could be largely eliminated by using a constant-distance mode of SECM imaging. This approach requires a distance-dependent signal and a feedback circuit, so that the tip could move up and down to remain at a constant distance from the imaged object. Different ways of doing it have been proposed including constant current mode,[154] tip position modulation,[155] the use of shear force-based feedback,[156,157] the AFM-SECM combination (see section 5.3), and tuning forks.[158,159] Schuhmann and co-workers applied constant-distance control based on an optical detection of shear forces to study vesicular release at single PC12 cell using SECM.[160] A carbon fiber microelectrode insulated by electrodeposition and dip-coating methods exhibited good stiffness and vibration characteristics for shear-force-based imaging. Topographic images of individual PC12 cells were obtained by recording the *z*-displacement during the scans, while the shear-force (and consequently the tip/cell distance) was set constant.

An alternative approach—to use the impedance of the SECM tip as the distance-dependent signal—was introduced by Horrocks *et al.*[161] and further developed by others.[58,162] The tip impedance is monitored by application of a high-frequency ac voltage bias between the tip and the auxiliary electrode, so that it can be separated from the lower frequency amperometric signals. By employing a piezo-based feedback controller, one can keep the impedance at a constant value and, thus, maintain a constant tip/substrate separation distance.[58] The imaging can take place directly in the cell growth media, and no redox mediator is required. Using this technique, Kurulugama *et al.*[163] obtained high quality constant-distance images of model neurons. The highest resolution was achieved using an ~1-μm-diameter carbon ring electrode (Fig. 15). In a somewhat related technique developed for biological imaging—scanning ion conductance microscopy—a pipette instead of a metal electrode was used as a scanning conductivity probe.[164] The use of nanometer-sized tips, which should become available for cellular SECM imaging within the next one or two years, may increase the lateral resolution from submicrometer range to about 10–20 nm.

5.5.2. Studies of redox enzymes, proteins, and DNA. The recent SECM studies of immobilized enzymes focused on two areas: measuring the catalytic enzyme activity and micropatterning the surface with enzymes. The use of two SECM-based approaches—generation/collection and feedback mode measurements—to probe redox enzymes (oxidoreductases) is illustrated in Fig. 16. The feedback mode (Fig. 16A) is more appropriate for high activity enzymes with a high surface coverage. The GC mode (Fig. 16B) is more sensitive and can be employed when enzyme kinetics are too slow for feedback measurements.

The earliest example of the feedback mode application is the study of catalytic oxidation of β-D-glucose to D-glucono-δ-lactone inside a micrometer-thick layer of immobilized glucose oxidase (GO) by Pierce *et al.*[165a] The oxidized form of the mediator produced by the diffusion-controlled tip reaction was reduced on the substrate surface by GO. Zero-order enzyme-mediator kinetics was established, and similar apparent

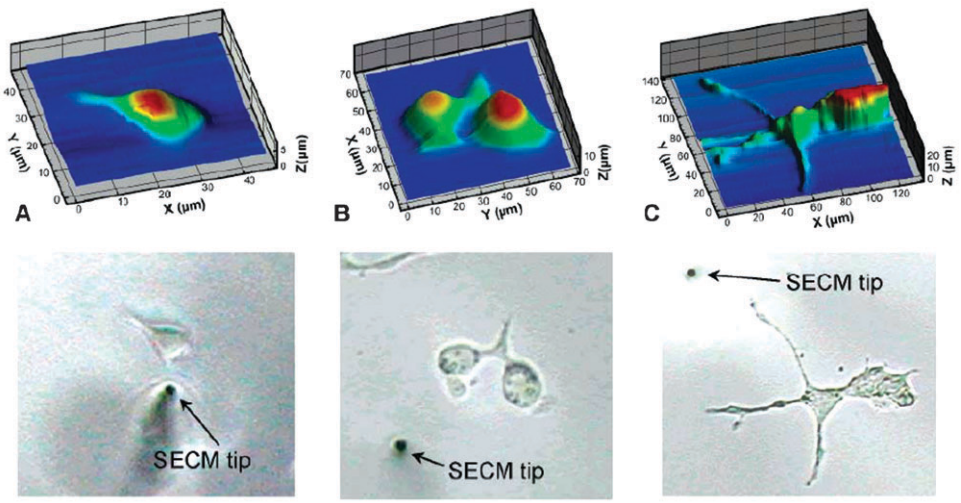

Fig. 15 Topographic images acquired using constant-impedance mode with a 1-μm carbon ring tip. (A) Undifferentiated PC12 cell; (B) PC12 cells in the early stage of neurite development following exposure to NGF; (C) differentiated PC12 cell. (Reprinted with permission from ref. 163. Copyrights 2005, American Chemical Society.)

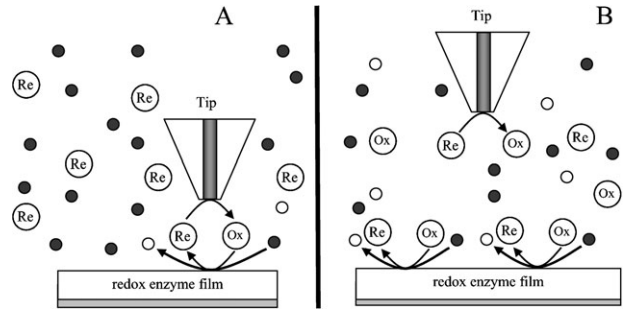

Fig. 16 Feedback and GC mode SECM measurements of enzyme kinetics. (A) Feedback mode: locally electrogenerated mediator is reduced by glucose (•) at the substrate surface; the reaction is catalyzed by glucose oxidase. (B) GC mode: the reduced form of the mediator is continuously produced by the enzyme-catalyzed reaction at the substrate and collected at the tip. The tip probes the concentration profile of reduced mediator species.

heterogeneous rate constants were measured for several mediators indicating saturation with respect to both β-D-glucose and mediator. A similar approach was used to observe the localized reaction of GO in the pores of track-etched polycarbonate membranes and membrane-bound NADH-Cytochrome C reductase in rat liver mitochondria.[165b]

The activity of immobilized alcohol dehydrogenase was probed and modified by changing the local pH.[166] The tip was positioned close to the enzyme film and used to increase the local pH by reducing water and producing hydroxide ions. A significant increase in enzyme activity was observed at higher pH. The opposite effect, *i.e.* local inactivation of the immobilized enzyme (diaphorase) by chlorine or bromine species electrogenerated at the tip, has also been reported.[167]

In a more recent study of the catalytic behavior of horseradish peroxidase (HRP), Zhou *et al.*[168] immobilized HRP onto glass using two methods. In the first method, the enzyme was immobilized by cross-linking with a copolymer on a glass slide. When placed in the buffer solution, the film swelled to form a hydrogel. In the second method, the same copolymer and avidin were co-immobilized on a glass slide, and biotin-labeled HRP was conjugated to the avidin in the film. The experiment was done in solution containing H_2O_2 and benzoquinone mediator. Hydroquinone was electrogenerated at the tip and catalytically reoxidized to benzoquinone by HRP in the presence of H_2O_2. This process produced positive SECM feedback. By varying the avidin loading of the film, the maximum feedback current was showed to be a linear function of the HRP surface concentration, and the detection limit of 7×10^5 HRP molecules within a 7-μm-diameter area was demonstrated.

The SECM was also used to fabricate and analyze micrometer-sized enzymatic structures on surfaces, which are potentially useful in the design of miniaturized biosensors. Wittstock and Schuhmann described the preparation and imaging of micrometer-sized spots of GO on Au.[169] First, the SECM tip was used to produce μm-sized defects in a self-assembled monolayer of dodecylthiolate on Au. Then, cystaminium dihydrochloride was adsorbed on the bare Au spots and used to covalently anchor periodate oxidized GO *via* Schiff base chemistry. H_2O_2 generated at the substrate was collected by the Pt tip in the SG/TC mode. Another approach to enzyme micropatterning was developed by Shiku *et al.*[170] who scanned a micropipette dispenser above the surface to create an array of 20-μm-sized solution droplets on a glass slide, from which micrometer-sized spots of active HRP were formed. A very recent application of the SECM to localized enzyme (GO) immobilization involved direct microspotting of polypyrrole–biotin films.[171] Ciobanu *et al.*[172] used a SAM film on a micro-patterned gold substrate to adsorb photosystem I (PSI). The selective adsorption of PSI onto hydroxyl-terminated thioalkane SAM ($HSC_{11}OH$) rather than the methyl-terminated SAM ($HSC_{11}CH_3$) was confirmed by SECM imaging.

The use of SECM to optimize the efficiency of "wired" enzyme electrodes has been reported.[173] In such devices, the enzymes are immobilized within a conductive polymer matrix on the electrode surface. The electrode efficiency depends on concentration of an enzyme in the polymer film and the ability of the matrix to recycle the enzyme by reducing/oxidizing it and shuttling the electrons to the electrode surface. SECM-based combinatorial screening techniques can reduce the time and the amounts of materials required for the optimization process. To probe the efficiency of wired bilirubin oxidase (BOD) and laccase (two enzymes catalyzing the ORR) electrodes, Fernández *et al.*[173] produced arrays of enzymatic spots on a glassy-carbon substrate surface. Each spot was made of a mixture of the enzyme and a conductive polymer and the mixture ratio was varied systematically within the array. Using the GC mode, a gold UME tip biased positively to produce O_2 from water was scanned above the enzymatic array. The authors found the optimal weight ratio for the two enzymes at which the oxygen reduction rate was close to the diffusion limit (Fig. 17). They ran the control experiments using a rotating disk electrode with the same mixture ratios and found the agreement between the two methods, although SECM measurements were ten times faster and required ~100,000 times less material.

SECM-based approaches to DNA studies and hybridization detection make use of inherent electrochemical properties of single and double stranded DNA and/or electroactive hybridization indicators, intercalating compounds, and redox labels. Wang *et al.*[174] introduced a method to visualize the surface-immobilized DNA by the generation/collection mode of SECM through the oxidation of guanine residues by tip-generated $Ru(bpy)_3^{3+}$. They also described silver-enhanced SECM imaging of DNA hybridization. Oligonucleotide probes at a microarray surface were hybridized with a biotinylated target, and the regions where sequence-specific hybridization had occurred were developed by the silver staining process.[175] The silver staining procedure formed locally conductive regions, which could produce positive SECM feedback. The related increase in the measured tip current made hybridized spots visible. In another report, DNA duplex regions were successfully visualized by SECM using ferrocenyl naphthalene diimide as intercalating hybridization indicator.[176]

Schuhmann *et al.*[177] proposed an electrostatic approach to detection of DNA hybridization. Since the DNA strands are

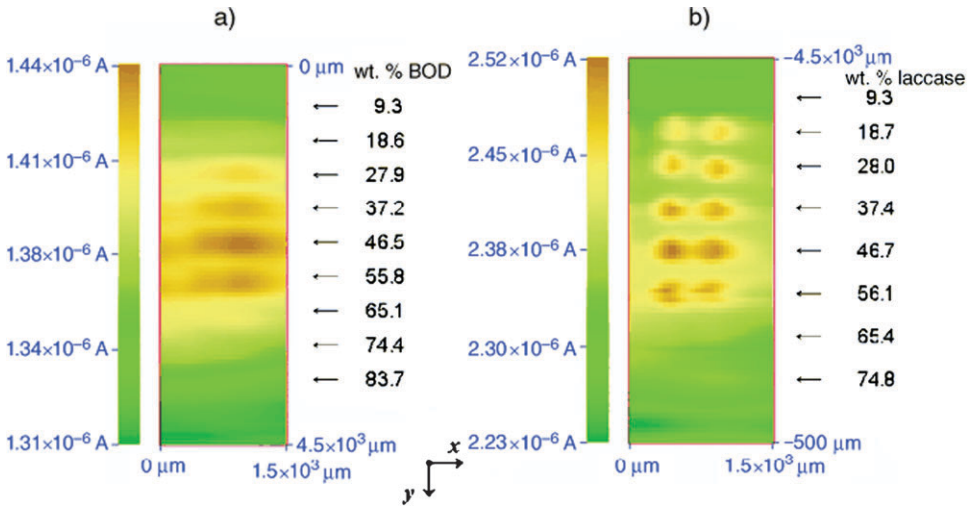

Fig. 17 SECM images of "wired" enzyme arrays containing spots with different polymer/enzyme ratios. (a) BOD (6.9 wt.% cross-linker) in pH 7.2 phosphate buffer, $i_T = -161$ nA, $E_s = 0.3$ V *versus* Ag/AgCl; (b) laccase (6.5 wt.% cross-linker) in pH 5.0 citrate buffer, $i_T = -240$ nA, $E_s = 0.4$ V *versus* Ag/AgCl. (Reprinted with permission from ref. 173. Copyright 2004, Wiley.)

negatively charged, the formation of double helices by complementary recognition processes can increase the density of negative charge and the extent of exclusion of a negatively charged redox species (*e.g.*, $Fe(CN)_6^{4-}$). This effect could be detected by SECM due to its capability to visualize small local variations in electrochemical reactivity with high spatial resolution. The charge transfer processes in DNA monolayers and their permeability to different redox mediators were also studied by Liu *et al.*[178]

The application of the SECM to protein detection has recently been reported by Girault group.[179] Using a detection scheme based on tagging adsorbed proteins with silver nanoparticles, the authors detected the quantity of protein as low as 0.1 ng which is comparable to state-of-the-art staining techniques. A positive feedback was obtained when a platinum tip approached the silver-tagged proteins in a 1mM $[Os(bpy)_3]^{2+}$ aqueous solution. $[Os(bpy)_3]^{3+}$ electrogenerated by the tip diffused toward the silver-tagged proteins and was reduced back to $[Os(bpy)_3]^{2+}$ thus forming the feedback loop.

5.5.3. Membrane transport. The transport of molecules across biological cell membranes, including planar bilayer lipid membranes (BLMs) and giant liposomes has been studied by SECM. The approaches used in those studies are similar to generation/collection and feedback SECM experiments. In the former mode, an amperometric tip is used to measure concentration profiles and monitor fluxes of molecules across the membrane. In a feedback-type experiment, the tip process depletes the concentration of the transferred species on one side of the membrane and in this way induces its transfer across the membrane.

Tsionsky *et al.* studied charge transport through the horizontally oriented BLM that separated the upper and lower compartments containing the same solution.[180] The bilayer was impermeable to hydrophilic ions like $Ru(NH_3)_6^{3+}$ and $Fe(CN)_6^{4-}$ and completely blocked ET between such species. However, the transmembrane ET current was observed when the BLM was doped by iodine. Using a similar experimental arrangement, Amemiya and Bard probed the transport of K^+ through gramicidin channels formed in horizontal BLMs.[181] The amperometric ion-selective micropipette electrodes used in those experiments were filled with a 10 mM valinomycin solution in 1,2-dichloroethane or 10 mM ETH 500. Both feedback and generation-collection modes were employed to investigate the transfer of K^+. In a somewhat similar manner, hydrophilic ion transfer through the voltage-gated channel formed in BLM by alamethicin was studied by Wilburn *et al.*[182] The pore formed by several alamethicin molecules was sufficiently large and hydrophilic to transport redox species such as $Ru(NH_3)_6^{3+}$ and $Fe(CN)_6^{3-}$, which could be detected by the Pt tip.

Two interesting examples of SECM studies of molecular transport across biological membranes were reported by Mauzeroll *et al.*[183,184] They measured the uptake of menadione by yeast cells and monitored its intracellular reaction with glutathione.[183] The export of the product of that reaction (thiodione) by ATP-dependent GS-X pumps is the way for a yeast cell to get rid of toxic menadione (Fig. 18). Because yeast cells are much smaller than either mammalian cells or purple bacteria used in other SECM studies, it was not possible to probe them individually. The average flux of about 30,000 thiodione molecules per second per cell was measured by a 1-µm-diameter tip, and numerical simulations were used to show that the overall process rate is limited by the uptake of menadione. The efflux through the GS-X pump was found to be at least an order of magnitude faster. In the second article,[184] the thiodione efflux from individual cells and groups of highly confluent hepatoblastoma (Hep G2) cells was probed by SG/TC experiments. The time evolution of concentration profiles was analyzed to determine the flux of 6.0×10^6 molecules per second per cell.

A novel application of SECM was to study transport processes across the nuclear envelope. Guo and Amemiya investigated the molecular transport facilitated by nuclear pore complexes (NPCs) in a large intact nucleus of

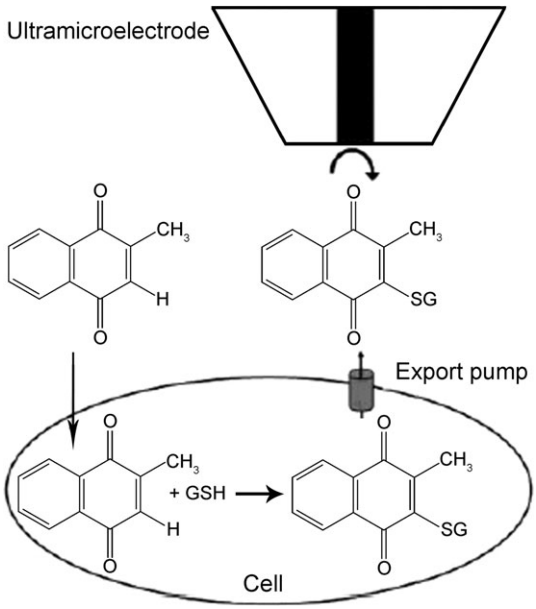

Fig. 18 Menadione-imposed oxidative stress on cells leads to the formation and excretion of thiodione into the extracellular media, where it can be detected by using SECM. (Reprinted with permission from ref. 183. Copyright 2000, National Academy of Sciences USA).

Xenopus laevis oocytes.[36] The NPC is a 60-120 MDa complex made of 30 or more distinct proteins. Small molecules can passively diffuse through it. The partitioning of redox species X across the nuclear envelope

$$\mathrm{X(outer\ solution)} \rightleftharpoons \mathrm{X(nucleus)} \qquad (20)$$

was characterized by obtaining approach curves and chronoamperograms. From such experiments performed with different mediators, the authors concluded that the nuclear envelope permeability is very high, and most NPCs on the nucleus are open. Estimates were obtained for the single-channel flux and the NPC diameter.

Most recently, Zhan and Bard used submicrometer-sized conical carbon fiber tips to approach, image, and puncture individual giant liposomes containing $Ru(bpy)_3^{2+}$.[37] The leakage of $Ru(bpy)_3^{2+}$ through the lipid membrane was observed. A higher stability of liposomes as compared to lipid bilayers allows one to perform measurements over a more extended period of time. Such "artificial cells" can be useful for studies of molecular transport and redox regulation of cellular processes. Amatore's group used microelectrodes in "artificial synapses" to probe the release of redox-active species by living cells in response to oxidative stress.[185]

6. Conclusions

The fast expansion of the SECM field during the last several years has been fueled by the introduction of new probes, commercially available instrumentation, and new practical applications. The fabrication of nanometer-sized tips and the development of numerous hybrid techniques have greatly enhanced the SECM capacity to solve problems in cell biology, surface science, and nanotechnology.

Acknowledgements

The support of our research in SECM by the National Science Foundation (CHE-0315558) and by the Donors of the Petroleum Research Fund administrated by the American Chemical Society is gratefully acknowledged.

References

1 G. Binnig and H. Rohrer, *Helv. Phys. Acta*, 1982, **55**, 726.
2 M. A. Dayton, J. C. Brown, K. J. Stutts and R. M. Wightman, *Anal. Chem.*, 1980, **52**, 946.
3 (*a*) R. C. Engstrom, M. Weber, D. J. Wunder, R. Burgess and S. Winguist, *Anal. Chem.*, 1986, **58**, 844; (*b*) R. C. Engstrom, T. Meaney, R. Tople and R. M. Wightman, *Anal. Chem.*, 1987, **59**, 2005.
4 C. W. Lin, F.-R. F. Fan and A. J. Bard, *J. Electrochem. Soc.*, 1987, **134**, 1038.
5 M. J. Heben, M. M. Dovek, N. S. Lewis, R. M. Penner and C. F. Quate, *J. Microsc.*, 1988, **152**, 651.
6 A. J. Bard, F.-R. F. Fan, J. Kwak and O. Lev, *Anal. Chem.*, 1989, **61**, 132.
7 J. Kwak and A. J. Bard, *Anal. Chem.*, 1989, **61**, 1221.
8 D. O. Wipf, *Bibliography for SECM papers and Closely Related Material*, http://www.msstate.edu/dept/Chemistry/dow1/secm/secm_bib.html.
9 *Scanning Electrochemical Microscopy*, ed. A. J. Bard and M. V. Mirkin, Marcel Dekker, New York, 2001.
10 A. L. Barker, M. Gonsalves, J. V. Macpherson, C. J. Slevin and P. R. Unwin, *Anal. Chim. Acta*, 1999, **385**, 223.
11 R. M. Wightman and D. O. Wipf, in *Electroanalytical Chemistry*, ed. A. J. Bard, Marcel Dekker, New York, Vol 15, 1988, p. 267.
12 C. Amatore, in *Physical Electrochemistry: Principles, Methods, and Application*, ed. I. Rubinstein, Marcel Dekker, New York, 1995, p. 131.
13 M. V. Mirkin, F.-R. F. Fan and A. J. Bard, *J. Electroanal. Chem.*, 1992, **328**, 47.
14 C. G. Zoski, B. Liu and A. J. Bard, *Anal. Chem.*, 2004, **76**, 3646.
15 Y. Selzer and D. Mandler, *Anal. Chem.*, 2000, **72**, 2383.
16 (*a*) S. Daniele, C. Bragato, I. Ciani and M. A. Baldo, *Electroanalysis*, 2003, **15**, 621; (*b*) J. Mauzeroll, E. A. Hueske and A. J. Bard, *Anal. Chem.*, 2003, **75**, 3880.
17 C. Demaille, M. B. Brust, M. Tsionsky and A. J. Bard, *Anal. Chem.*, 1997, **69**, 2323.
18 Y. Lee, S. Amemiya and A. J. Bard, *Anal. Chem.*, 2001, **73**, 226.
19 P. Liljeroth, C. Johans, C. J. Slevin, B. M. Quinn and K. Kontturi, *Anal. Chem.*, 2002, **74**, 1972.
20 J. V. Macpherson and P. R. Unwin, *Anal. Chem.*, 2000, **72**, 276.
21 A. J. Bard and L. R. Faulkner, *Electrochemical Methods*, Wiley, New York, 2001.
22 P. R. Unwin and A. J. Bard, *J. Phys. Chem.*, 1991, **95**, 7814.
23 F. Zhou, P. R. Unwin and A. J. Bard, *J. Phys. Chem.*, 1992, **96**, 4917.
24 F. Zhou and A. J. Bard, *J. Am. Chem. Soc.*, 1994, **116**, 393.
25 D. A. Treichel, M. V. Mirkin and A. J. Bard, *J. Phys. Chem.*, 1994, **98**, 5751.
26 P. R. Unwin, A. J. Bard and C. Demaille, *J. Phys. Chem.*, 1996, **100**, 14137.
27 N. Baltes, L. Thouin, C. Amatore and J. Heinze, *Angew. Chem., Int. Ed.*, 2004, **43**, 1431.
28 G. Denuault, M. H. Troise-Frank and L. M. Peter, *Faraday Discuss.*, 1992, **94**, 23.
29 B. R. Horrocks, M. V. Mirkin, D. T. Pierce, A. J. Bard, G. Nagy and K. Toth, *Anal. Chem.*, 1993, **65**, 1213.
30 C. Wei, A. J. Bard, G. Nagy and K. Toth, *Anal. Chem.*, 1995, **67**, 1346.
31 C. Wei, A. J. Bard, I. Kapui, G. Nagy and K. Toth, *Anal. Chem.*, 1996, **68**, 2651.

32 E. Klusmann and J. W. Schultze, *Electrochim. Acta*, 1997, **42**, 3123.
33 R. D. Martin and P. R. Unwin, *Anal. Chem.*, 1998, **70**, 276.
34 M. V. Mirkin, F.-R. F. Fan and A. J. Bard, *Science*, 1992, **257**, 364.
35 F.-R. F. Fan, M. V. Mirkin and A. J. Bard, *J. Phys. Chem.*, 1994, **98**, 1475.
36 J. Guo and S. Amemiya, *Anal. Chem.*, 2005, **77**, 2147.
37 W. Zhan and A. J. Bard, *Anal. Chem.*, 2006, **78**, 726.
38 P. Sun, C. Cai and M. V. Mirkin, manuscript in preparation.
39 Y. H. Shao and M. V. Mirkin, *J. Electroanal. Chem.*, 1997, **439**, 137.
40 Y. H. Shao and M. V. Mirkin, *J. Phys. Chem. B*, 1998, **102**, 9915.
41 Z. Zhang, Y. Yuan, P. Sun, B. Su, J. Guo, Y. Shao and H. H. Girault, *J. Phys. Chem. B*, 2002, **106**, 6713.
42 M. V. Mirkin and M. Tsionsky, in *Scanning Electrochemical Microscopy*, ed. A. J. Bard and M. V. Mirkin, Marcel Dekker, New York, 2001, p. 299.
43 F. O. Laforge, T. Kakiuchi, F. Shigematsu and M. V. Mirkin, *J. Am. Chem. Soc.*, 2004, **126**, 15380.
44 P. Sun, F. Li, Y. Chen, M. Q. Zhang, Z. Q. Zhang, Z. Gao and Y. Shao, *J. Am. Chem. Soc.*, 2003, **125**, 9600.
45 B. M. Quinn, P. Liljeroth, V. Ruiz, T. Laaksonen and K. Kontturi, *J. Am. Chem. Soc.*, 2003, **125**, 6644.
46 D. G. Georganopoulou, M. V. Mirkin and R. W. Murray, *Nano Lett.*, 2004, **4**, 1763.
47 P. Sun, Z. Zhang, Z. Gao and Y. Shao, *Angew. Chem., Int. Ed.*, 2002, **41**, 3445.
48 J. Zhang, J. Strutwolf, S. Cannan and P. R. Unwin, *Electrochem. Commun.*, 2003, **5**, 105.
49 I. Ciani and S. Daniele, *Anal. Chem.*, 2004, **76**, 6575.
50 L. A. Nagahara, T. Tundat and S. M. Lindsay, *Rev. Sci. Instrum.*, 1989, **60**, 3128.
51 P. Sun, Z. Zhang, J. Guo and Y. Shao, *Anal. Chem.*, 2001, **73**, 5346.
52 C. J. Slevin, N. J. Gray, J. V. Macpherson, M. A. Webb and P. R. Unwin, *Electrochem. Commun.*, 1999, **1**, 282.
53 C. Kranz, G. Friedbacher, B. Mizaikoff, A. Lugstein, J. Smoliner and E. Bertagnolli, *Anal. Chem.*, 2001, **73**, 2491.
54 P. Sun and M. V. Mirkin, *Anal. Chem.*, 2006, **78**, 6526.
55 Y. Shao, M. V. Mirkin, G. Fish, S. Kokotov, D. Palanker and A. Lewis, *Anal. Chem.*, 1997, **69**, 1627.
56 B. B. Katemann and W. Schuhmann, *Electroanalysis*, 2002, **14**, 22.
57 D. O. Wipf, A. C. Michael and R. M. Wightman, *J. Electroanal. Chem.*, 1989, **269**, 15.
58 M. A. Alpuche-Aviles and D. O. Wipf, *Anal. Chem.*, 2001, **73**, 4873.
59 M. V. Mirkin, in *Scanning Electrochemical Microscopy*, ed. A. J. Bard and M. V. Mirkin, Marcel Dekker, New York, 2001, p. 145.
60 M. Arca, A. J. Bard, B. R. Horrocks, T. C. Richards and D. A. Treichel, *Analyst*, 1994, **119**, 719.
61 A. J. Bard, F.-R. F. Fan and M. V. Mirkin, in *Electroanalytical Chemistry*, ed. A. J. Bard, Marcel Dekker, New York, vol. 18, 1993, p. 243.
62 A. J. Bard, F.-R. F. Fan, D. T. Pierce, P. R. Unwin, D. O. Wipf and F. Zhou, *Science*, 1991, **254**, 68.
63 A. J. Bard, M. V. Mirkin, P. R. Unwin and D. O. Wipf, *J. Phys. Chem.*, 1992, **96**, 1861.
64 C. Lefrou, *J. Electroanal. Chem.*, 2006, **592**, 103.
65 J. L. Amphlett and G. Denuault, *J. Phys. Chem. B*, 1998, **102**, 9946.
66 C. Wei, A. J. Bard and M. V. Mirkin, *J. Phys. Chem.*, 1995, **99**, 16033.
67 M. Tsionsky, A. J Bard and M. V. Mirkin, *J. Phys. Chem.*, 1996, **100**, 17881.
68 M. Tsionsky, A. J. Bard and M. V. Mirkin, *J. Am. Chem. Soc.*, 1997, **119**, 10785.
69 (*a*) B. Liu, A. J. Bard, M. V. Mirkin and S. E. Creager, *J. Am. Chem. Soc.*, 2004, **126**, 1485; (*b*) H. Yamada, M. Ogata and T. Koike, *Langmuir*, 2006, **22**, 7923.
70 B. Liu, S. A. Rotenberg and M. V. Mirkin, *Proc. Natl. Acad. Sci. U. S. A.*, 2000, **97**, 9855.
71 B. Liu, S. A. Rotenberg and M. V. Mirkin, *Anal. Chem.*, 2002, **74**, 6340.
72 C. Cai, B. Liu, M. V. Mirkin, H. A. Frank and J. F. Rusling, *Anal. Chem.*, 2002, **74**, 114.
73 W. Feng, S. A. Rotenberg and M. V. Mirkin, *Anal. Chem.*, 2003, **75**, 4148.
74 E. R. Scott and H. S. White, *Anal. Chem.*, 1993, **65**, 1537.
75 B. D. Bath, R. D. Lee, H. S. White and E. R. Scott, *Anal. Chem.*, 1998, **70**, 1047.
76 M. H. Troise-Frank and G. Denuault, *J. Electroanal. Chem.*, 1993, **354**, 331.
77 M. H. Troise-Frank and G. Denuault, *J. Electroanal. Chem.*, 1994, **379**, 405.
78 B. R. Horrocks and M. V. Mirkin, *J. Chem. Soc., Faraday Trans.*, 1998, **94**, 1115.
79 H. Xiong, J. Guo, K. Kurihara and S. Amemiya, *Electrochem. Commun.*, 2004, **6**, 615.
80 Q. Fulian, A. C. Fisher and G. Denuault, *J. Phys. Chem. B*, 1999, **103**, 4387.
81 O. Sklyar and G. Wittstock, *J. Phys. Chem. B*, 2002, **106**, 7499.
82 O. Sklyar, A. Kueng, C. Kranz, B. Mizaikoff, A. Lugstein, E. Bertagnolli and G. Wittstock, *Anal. Chem.*, 2005, **77**, 764.
83 O. Sklyar, M. Träuble, C. Zhao and G. Wittstock, *J. Phys. Chem. B*, 2006, **110**, 15869.
84 M. V. Mirkin, T. C. Richards and A. J. Bard, *J. Phys. Chem.*, 1993, **97**, 7672.
85 M. V. Mirkin, L. O. S. Bulhões and A. J. Bard, *J. Am. Chem. Soc.*, 1993, **115**, 201.
86 W. J. Miao, Z. F. Ding and A. J. Bard, *J. Phys. Chem. B*, 2002, **106**, 1392.
87 D. O. Wipf and A. J. Bard, *J. Electrochem. Soc.*, 1991, **138**, 469.
88 Y. Selzer, I. Turyan and D. Mandler, *J. Phys. Chem. B*, 1999, **103**, 1509.
89 J. Zhou, Y. Zu and A. J. Bard, *J. Electroanal. Chem.*, 2000, **491**, 22.
90 S. Jayaraman and A. C. Hillier, *J. Combinat. Chem.*, 2004 **6**, 27.
91 M. Black, J. Cooper and P. McGinn, *Meas. Sci. Technol.*, 2005, **16**, 174.
92 A. R. Kucernak, P. B. Chowdhury, C. P. Wilde, G. H. Kelsall, Y. Y. Zhu and D. E. Williams, *Electrochim. Acta*, 2000, **45**, 4483.
93 J. Fernández and A. J. Bard, *Anal. Chem.*, 2003, **75**, 2967.
94 E. Reddington, A. Sapienza, B. Gurau, R. Viswanathan, S. Sarangapani, E. S. Smotkin and T. E. Mallouk, *Science*, 1998, **280**, 1735.
95 J. Fernández, D. A. Walsh and A. J. Bard, *J. Am. Chem. Soc.*, 2005, **127**, 357.
96 J. Fernández, V. Raghuveer, A. Manthiram and A. J. Bard, *J. Am. Chem. Soc.*, 2005, **127**, 13100.
97 Y. C. Weng, F.-R. F. Fan and A. J. Bard, *J. Am. Chem. Soc.*, 2005, **127**, 17576.
98 S. Jayaraman and A. C. Hillier, *Langmuir*, 2001, **17**, 7857.
99 S. Jayaraman and A. C. Hillier, *J. Phys. Chem. B*, 2003, **107**, 5221.
100 J. Zhang, C. J. Slevin, C. Morton, P. Scott, D. J. Walton and P. R. Unwin, *J. Phys. Chem. B*, 2001, **105**, 11120.
101 A. P. O'Mullane, J. V. Macpherson, J. Cervera-Montesinos, J. A. Manzanares, F. Frehill, J. G. Vos and P. R. Unwin, *J. Phys. Chem. B*, 2004, **108**, 7219–7227.
102 A. L. Whitworth, D. Mandler and P. R. Unwin, *Phys. Chem. Chem. Phys.*, 2005, **7**, 356.
103 G. Shi, L. F. Garfias-Mesias and W. H. Smyrl, *J. Electrochem. Soc.*, 1998, **145**, 3011.
104 D. E. Cliffel and A. J. Bard, *Anal. Chem.*, 1998, **70**, 1993.
105 B. Gollas, P. N. Bartlett and G. Denuault, *Anal. Chem.*, 2000, **72**, 349.
106 C. Xiang, Q. Xie, J. Hu and S. Yao, *J. Electroanal. Chem.*, 2005, **584**, 201.
107 E. Fortin, Y. Defontaine, P. Mailley, T. Livache and S. Szunerits, *Electroanalysis*, 2005, **17**, 5.
108 F.-M. Boldt, J. Heinze, M. Diez, J. Petersen and M. Bolrsch, *Anal. Chem.*, 2004, **76**, 3473.
109 F.-R. F. Fan, D. Cliffel and A. J. Bard, *Anal. Chem.*, 1998, **70**, 2941.
110 C. E. Gardner and J. V. Macpherson, *Anal. Chem.*, 2002, **74**, 576A.
111 J. V. Macpherson and P. R. Unwin, *Anal. Chem.*, 2001, **73**, 550.

112 J. Abbou, C. Demaille, M. Dret and J. Moiroux, *Anal. Chem.*, 2002, **74**, 6355.
113 J. Abbou, A. Anne and C. Demaille, *J. Am. Chem. Soc.*, 2004, **126**, 10095.
114 A. Lugstein, E. Bertagnolli, C. Kranz, A. Kueng and B. Mizaikoff, *Appl. Phys. Lett.*, 2002, **81**, 349.
115 D. P. Burt, N. R. Wilson, P. S. Dobson, J. M. R. Weaver and J. V. Macpherson, *Nano Lett.*, 2005, **5**, 639.
116 N. R. Wilson, D. H. Cobden and J. V. Macpherson, *J. Phys. Chem. B*, 2002, **106**, 13102.
117 R. J. Fasching, Y. Tao and F. B. Prinz, *Sens. Actuators, B*, 2005, **108**, 964.
118 P. S. Dobson, J. M. R. Weaver, M. N. Holder, P. R. Unwin and J. V. Macpherson, *Anal. Chem.*, 2005, **77**, 424.
119 (*a*) J. V. Macpherson, P. R. Unwin, A. C. Hillier and A. J. Bard, *J. Am. Chem. Soc.*, 1996, **118**, 6445; (*b*) C. E. Jones, J. V. Macpherson and P. R. Unwin, *J. Phys. Chem. B*, 2000, **104**, 2351.
120 C. J. Boxley, H. S. White, C. E. Gardner and J. V. Macpherson, *J. Phys. Chem. B*, 2003, **107**, 9677.
121 J. V. Macpherson, C. E. Jones, A. L. Baker and P. R. Unwin, *Anal. Chem.*, 2002, **74**, 1841.
122 K. B. Holt, A. J. Bard, Y. Show and G. M. Swain, *J. Phys. Chem. B*, 2004, **108**, 15117.
123 J. V. Macpherson and J. L. Delplancke, *J. Electrochem. Soc.*, 2002, **149**, B306.
124 A. Davoodi, J. Pan, C. Leygraf and S. Norgren, *Electrochem. Solid State Lett.*, 2005, **8**, B21.
125 C. Kranz, A. Kueng, A. Lugstein, E. Bertagnolli and B. Mizaikoff, *Ultramicroscopy*, 2004, **100**, 127.
126 Y. Hirata, S. Yabuki and F. Mizutani, *Bioelectrochemistry*, 2004, **63**, 217.
127 C. E. Gardner, P. R. Unwin and J. V. Macpherson, *Electrochem. Commun.*, 2005, **7**, 612.
128 M. N. Holder, C. E. Gardner, J. V. Macpherson and P. R. Unwin, *J. Electroanal. Chem.*, 2005, **585**, 8.
129 P. A. Kottke and A. G. Fedorov, *J. Electroanal. Chem.*, 2005, **583**, 221.
130 D. H. Craston, C. W. Lin and A. J. Bard, *J. Electrochem. Soc.*, 1988, **135**, 785.
131 D. Mandler and A. J. Bard, *J. Electrochem. Soc.*, 1989, **136**, 3143.
132 O. E. Hüsser, D. H. Craston and A. J. Bard, *J. Vac. Sci. Technol., B*, 1988, **6**, 1873.
133 O. E. Hüsser, D. H. Craston and A. J. Bard, *J. Electrochem. Soc.*, 1989, **136**, 3222.
134 Y.-M. Wuu, F.-R. F. Fan and A. J. Bard, *J. Electrochem. Soc.*, 1989, **136**, 885.
135 F. Forouzan and A. J. Bard, *J. Phys. Chem. B*, 1997, **101**, 10876.
136 D. Mandler and A. J. Bard, *J. Electrochem. Soc.*, 1990, **137**, 2468.
137 D. Mandler and A. J. Bard, *J. Electrochem. Soc.*, 1990, **137**, 1079.
138 I. Shohat and D. Mandler, *J. Electrochem. Soc.*, 1994, **141**, 995.
139 K. Borgwarth, C. Ricken, D. G. Ebling and J. Heinze, *Ber. Bunsen-Ges. Phys. Chem.*, 1995, **99**, 1421.
140 C. Heß, K. Borgwarth, C. Ricken, D. G. Ebling and J. Heinze, *Electrochim. Acta*, 1997, **42**, 3065.
141 A. K. Neufeld, A. P. O'Mullane and A. M. Bond, *J. Am. Chem. Soc.*, 2005, **127**, 13846.
142 (*a*) Y. Yatziv, I. Turyan and D. Mandler, *J. Am. Chem. Soc.*, 2002, **124**, 5618; (*b*) I. Turyan, M. Etienne, D. Mandler and W. Schuhmann, *Electroanalysis*, 2005, **17**, 5.
143 C. Combellas and F. Kanoufi, *J. Electroanal. Chem.*, 2006, **589**, 243, and references cited therein.
144 C. Lee, J. Kwak and A. J. Bard, *Proc. Natl. Acad. Sci. U. S. A.*, 1990, **87**, 1740.
145 R. K Zhu, S. M. Macfie and Z. F. Ding, *J. Exp. Bot.*, 2005, **56**, 2831.
146 K. B. Holt and A. J. Bard, *Biochemistry*, 2005, **44**, 13214.
147 T. Yasukawa, T. Kaya and T. Matsue, *Electroanalysis*, 2000, **12**, 653.
148 Y.-S. Torisawa, T. Kaya, Y. Takii, D. Oyamatsu, M. Nishizawa and T. Matsue, *Anal. Chem.*, 2003, **75**, 2154.
149 H. Shiku, T. Shiraishi, H. Ohya, T. Matsue, H. Abe, H. Hoshi and M. Kobayashi, *Anal. Chem.*, 2001, **73**, 3751.
150 Y. Takii, K. Takoh, M. Nishizawa and T. Matsue, *Electrochim. Acta*, 2003, **48**, 3381.
151 F. Longobardi, P. Cosma, F. Milano, A. Agostiano, J. Mauzeroll and A. J. Bard, *Anal. Chem.*, 2006, **78**, 5046.
152 B. Liu, W. Cheng, S. A. Rotenberg and M. V. Mirkin, *J. Electroanal. Chem.*, 2001, **500**, 590.
153 J. M. Liebetrau, H. M. Miller, J. E. Baur, S. A. Takacs, V. Anupunpisit, P. A. Garris and D. O. Wipf, *Anal. Chem.*, 2003, **75**, 563.
154 D. O. Wipf, A. J. Bard and D. E. Tallman, *Anal. Chem.*, 1993, **65**, 1373.
155 D. O. Wipf and A. J. Bard, *Anal. Chem.*, 1992, **64**, 1362.
156 A. Hengstenberg, C. Kranz and W. Schuhmann, *Chem.–Eur. J.*, 2000, **6**, 1547.
157 (*a*) B. B. Katemann, A. Schulte and W. Schuhmann, *Chem.–Eur. J.*, 2003, **9**, 2025; (*b*) B. B. Katemann, A. Schulte and W. Schuhmann, *Electroanalysis*, 2004, **16**, 60.
158 P. I. James, L. F. Garfias-Mesias, P. J. Moyer and W. H. Smyrl, *J. Electrochem. Soc.*, 1998, **145**, L64.
159 Y. Lee, Z. F. Ding and A. J. Bard, *Anal. Chem.*, 2002, **74**, 3634.
160 A. Hengstenberg, A. Blöchl, I. D. Dietzel and W. Schuhmann, *Angew. Chem., Int. Ed.*, 2001, **40**, 905.
161 B. R. Horrocks, D. Schmidtke, A. Heller and A. J. Bard, *Anal. Chem.*, 1993, **65**, 3605.
162 C. Gabrielli, F. Huet, M. Keddam, P. Rousseau and V. Vivier, *J. Phys. Chem. B*, 2004, **108**, 11620.
163 R. T. Kurulugama, D. O. Wipf, S. A. Takacs, S. Pongmayteegul, P. A. Garris and J. E. Baur, *Anal. Chem.*, 2005, **77**, 1111.
164 Y. E. Korchev, C. L. Bashford, M. Milovanovic, I. Vodyanoy and M. J. Lab, *Biophys. J.*, 1997, **7**, 653.
165 (*a*) D. T. Pierce, P. R. Unwin and A. J. Bard, *Anal. Chem.*, 1992, **64**, 1795; (*b*) D. T. Pierce and A. J. Bard, *Anal. Chem.*, 1993, **65**, 3598.
166 J. C. O'Brien, J. Shumaker-Parry and R. C. Engstrom, *Anal. Chem.*, 1998, **70**, 1307.
167 H. Shiku, T. Takeda, H. Yamada, T. Matsue and I. Uchida, *Anal. Chem.*, 1995, **67**, 312.
168 J. Zhou, C. Campbell, A. Heller and A. J. Bard, *Anal. Chem.*, 2002, **74**, 4007.
169 G. Wittstock and W. Schuhmann, *Anal. Chem.*, 1997, **69**, 5059.
170 H. Shiku, T. Matsue and I. Uchida, *Anal. Chem.*, 1996, **68**, 1276.
171 S. A. G. Evans, K. Brakha, M. Billon, P. Mailley and G. Denuault, *Electrochem. Commun.*, 2005, **7**, 135.
172 M. Ciobanu, H. A. Kincaid, G. K. Jennings and D. E. Cliffel, *Langmuir*, 2005, **21**, 692.
173 J. L. Fernández, N. Mano, A. Heller and A. J. Bard, *Angew. Chem., Int. Ed.*, 2004, **43**, 6355.
174 J. Wang and F. M. Zhou, *J. Electroanal. Chem.*, 2002, **537**, 95.
175 J. Wang, F. Y. Song and F. M. Zhou, *Langmuir*, 2002, **18**, 6653.
176 K. Yamashita, M. Takagi, K. Uchida, H. Kondo and S. Takenaga, *Analyst*, 2001, **126**, 1210.
177 (*a*) F. Turcu, A. Schulte, G. Hartwich and W. Schuhmann, *Biosens. Bioelectron.*, 2004, **20**, 925; (*b*) F. Turcu, A. Schulte, G. Hartwich and W. Schuhmann, *Angew. Chem., Int. Ed.*, 2004, **43**, 3482.
178 B. Liu, A. J. Bard, C. Z. Li and H. B. Kraatz, *J. Phys. Chem. B*, 2005, **109**, 5193.
179 (*a*) M. Carano, N. Lion, J. Abid and H. H. Girault, *Electrochem. Commun.*, 2004, **6**, 1217; (*b*) M. Carano, N. Lion and H. H. Girault, *Chimia*, 2005, **59**, 105.
180 M. Tsionsky, J. Zhou, S. Amemiya, F.-R. F. Fan, A. J. Bard and R. A. W. Dryfe, *Anal. Chem.*, 1999, **71**, 4300.
181 S. Amemiya and A. J. Bard, *Anal. Chem.*, 2000, **72**, 4940.
182 J. P. Wilburn, D. W. Wright and D. E. Cliffel, *Analyst*, 2006, **131**, 311.
183 J. Mauzeroll and A. J. Bard, *Proc. Natl. Acad. Sci. U. S. A.*, 2004, **101**, 7862.
184 J. Mauzeroll, A. J. Bard, O. Owhadian and T. J. Monks, *Proc. Natl. Acad. Sci. U. S. A.*, 2004, **101**, 17582.
185 C. Amatore, S. Arbault, D. Bruce, P. de Oliveira, M. Erard and M. Vuillaume, *Faraday Discuss.*, 2000, **116**, 319.